High precision numerical sequences of rotating hairy black holes

Gustavo García,[1,*] Eric Gourgoulhon,[2,†] Philippe Grandclément,[2,‡] and Marcelo Salgado[1,§]

[1]*Instituto de Ciencias Nucleares, Universidad Nacional Autónoma de México, A.P. 70-543, CDMX 04510, Mexico*

[2]*Laboratoire Univers et Théories, Observatoire de Paris, Université PSL, Université Paris Cité, UMR 8102 CNRS, F-92190 Meudon, France*

(Received 13 February 2023; accepted 23 March 2023; published 28 April 2023)

We analyze numerically the existence of regular stationary rotating hairy black holes within the framework of general relativity, which are the result of solving the Einstein-Klein-Gordon system for a complex-valued scalar field under suitable boundary (regularity and asymptotically flat) conditions. To that aim we solve the corresponding system of elliptic partial differential equations using spectral methods which are specially suited for such a numerical task. In order to obtain such system of equations we employ a parametrization for the metric that corresponds to quasi-isotropic coordinates (QIC) that have been used in the past for analyzing different kinds of stationary rotating relativistic systems. Our findings are in agreement with those reported originally by Herdeiro and Radu. The method is submitted to several analytic and numerical tests, which include the recovery of the Kerr solution in QIC and the cloud solutions in the Kerr background. We report different global quantities that allow us to determine the contribution of the boson hair to the spacetime, as well as relevant quantities at the horizon, like the surface gravity. The latter indicates to what extent the hairy solutions approach the extremal limit, noting that for this kind of solutions the ratio of the angular momentum per squared mass $J_\infty/M^2_{\rm ADM}$ can be larger than unity due to the contribution of the scalar hair, a situation which differs from the Kerr metric where this parameter is bounded according to $0 \leq |J/M^2| \leq 1$, with the upper bound corresponding to the extremal case.

DOI: 10.1103/PhysRevD.107.084047

I. INTRODUCTION

Black holes (BH) are one of the most fascinating predictions of general theory of relativity (GR). A BH region within an asymptotically flat (AF) spacetime is a no-escape region where the event horizon, $\mathcal{H}^+$, a null surface, separates this region from the "observable universe," called the domain of outer communication (DOC).

Uniqueness theorems establish that the only regular, AF and stationary BH in GR coupled to Maxwell theory, are contained within the Kerr-Newman family of solutions which are characterized by only three parameters, the mass, electric charge and angular momentum [1]. In particular, in the absence of rotation, this family reduces to the Reissner-Nordstrom BH, and for a vanishing electric charge the only possible solution is the Schwarzschild solution, which has only the mass as a single parameter.

The no-hair conjecture, first proposed by Carter in 1968 [2], stipulates that the only stationary AFBH are precisely described in terms of those three parameters. This conjecture has been reinforced by no-hair theorems which establish the circumstances under which some nontrivial fields cannot coexist outside a BH [3–5]. Similar theorems are extended as to include nonminimally coupled scalar fields to gravity [6]. Several of these "no-go theorems" are mainly restricted to static, spherically symmetric and asymptotically flat scenarios, leading to the conclusion that the only possible BH corresponds to the Schwarzschild solution.

From the observational point of view, there is strong, albeit indirect evidence, that BH's do exist in the universe. For instance, the gravitational-wave (GW) observatories LIGO-VIRGO together with massive numerical simulations and a detailed statistical analysis indicate that the source of several GW signals detected in recent years come from the collision of two BH that presumably are of Kerr or Schwarzschild type [7]. Moreover, the dynamics of stars near the center of our galaxy (Sgr A*) also shows that the central object is undoubtedly a supermassive BH [8,9]. Finally, the Event Horizon Telescope (EHT) has produced radio images from the matter in the neighborhood of the center of galaxy M87 and our own galaxy that are consistent with the hypothesis of an accretion luminous disk around a Kerr BH [10], which is in addition, one of the simple mechanisms to explain the emission of relativistic jets in this kind of environments [11].

*gustavo.garcia@correo.nucleares.unam.mx
†eric.gourgoulhon@obspm.fr
‡Philippe.Grandclement@obspm.fr
§marcelo@nucleares.unam.mx

This overwhelming observational evidence about the existence of BH's in the universe leaves, however, some room for speculating about the specific kind of BH that have been observed, notably, BH's other than Kerr or Schwarzschild. At this respect, we mention that despite the elaboration of several no-hair theorems, hairy BH solutions have been found in different kind of field theories coupled to GR [12,13] (for a review see [14,15]), showing that more general BH's require more parameters and thus, indicating that the no-hair conjecture might be wrong. Nevertheless, most, if not all, of those kind of hairy BH solutions have proved to be unstable under linear perturbations (cf. Refs. [13,16]), and correspond to static and spherically symmetric situations. Thus, it is possible that if the stability condition is included the no-hair conjecture may hold.

In 2014 a remarkable result that puts in jeopardy this conjecture was obtained by Herdeiro and Radu [17,18] (hereafter referred to as HR): Namely, that a regular, stationary and rotating AFBH solution in GR can coexist with a complex-valued boson field (hereafter hairy solutions). This is a surprising result in view that a specific no-hair theorem for this kind of matter was proved in the past, although assuming a static and spherically symmetric spacetime [5]. The hairy solutions found by HR under different kind of values for the boundary conditions at the horizon are numerical, and the corresponding partial differential equations (PDEs) involved in the problem are not easy to solve, even numerically. The authors also showed that nontrivial configurations for the same kind of fields can be also found when the background is fixed, notably, a Kerr spacetime background. These solutions were termed *clouds*. The numerical analysis of these clouds was then extended as to include electric charge, and nontrivial charged scalar clouds were also found within a fixed Kerr-Newman background [19].

A further study by some of us pinpointed the reason of why the no-hair theorems for static situations could not be extended to stationary and rotating scenarios [20,21]. This analysis provides a further hint to understand in a simple and heuristic fashion the existence of those cloud solutions.

It is still premature to assess the impact of those hairy solutions from the observational point of view, as the current data from the observations alluded above have several uncertainties, which in the future might be accommodated as to include or rule out this kind of hairy black holes. Theoretically, these hairy solutions might be unstable but they still cannot be dismissed since a sound stability analysis is still lacking. Only a preliminary analysis of this sort has been performed recently [22,23], but it only includes a very small region of the parameter space of solutions. Other hairy solutions in alternative gravity theories have also been found [15,24]. Thus, observations can also validate, rule out or constrain those solutions as well, or the alternative theories themselves [25].

Since the hairy solutions found by HR might have an impact in the interpretation of the forthcoming observations regarding BH's, it is important to provide an independent study of this kind of solutions.

The goal of this paper is to provide that analysis using an approach that differs significantly from the HR method. Namely, (a) we use a parametrization of the metric in terms of quasi-isotropic coordinates (QIC), that leads to a rather compact system of elliptic PDE for the metric potentials; and (b) we use a spectral method decomposition that has proved to be well suited to solve those kind of PDEs with great numerical precision.[1] Spectral methods have been used systematically in the past by the Meudon group and collaborators [27] to analyze numerically a large variety of scenarios involving similar kind of relativistic rotating systems, like neutron stars, boson stars, Galileon BH's, among others. Thus, these numerical methods are reliable and relatively easy to implement thanks to the spectral-method library KADATH [28]. Furthermore, other groups have used KADATH to construct a large variety of isolated and binary initial data to explore and analyze compact-object binaries [29].

The article is organized as follows. In Sec. II we provide the formalism and equations. Section II A discusses the boundary conditions; Sec. III introduces some formulas to compute global quantities associated with the BH solutions, like the Komar mass, angular momentum, and the surface gravity. Section IV provides the numerical analysis and Sec. V compares our results with previous studies reported recently by HR. Finally, in Sec. VI we present the conclusions and outlook for further studies along this line of research. Several appendixes are included in order to complete the different sections and to make the article more self-contained.

II. FORMALISM AND FIELD EQUATIONS

We consider the action functional

$$S[g_{ab},\Psi]=\int\left\{\frac{R}{16\pi}-\left[\frac{1}{2}(\nabla_c\Psi^*)(\nabla^c\Psi)+\frac{1}{2}\mu^2\Psi^*\Psi\right]\right\}\times\sqrt{-g}d^4x, \tag{1}$$

associated with GR and a matter contribution from a complex-valued scalar field Ψ, submitted to a potential that includes only a mass term. Variation of the metric and the scalar field leads respectively to Einstein's field equations endowed with an energy-momentum tensor (EMT) that

[1]At the time this work was completed we became aware about Ref. [26] where the authors analyze different kind of BH's using spectral methods and perform similar sort of tests that appear in our Appendix A.

describes the distribution of the scalar field, and a Klein-Gordon equation for the field:

$$G_{ab} = R_{ab} - \frac{1}{2} g_{ab} R = 8\pi T_{ab}, \tag{2}$$

$$T_{ab} = \nabla_{(a}\Psi^{*}\nabla_{b)}\Psi - g_{ab}\left[\frac{1}{2}(\nabla_{c}\Psi^{*})(\nabla^{c}\Psi) + \frac{1}{2}\mu^{2}\Psi^{*}\Psi\right] \tag{3}$$

$$\Box\Psi = \mu^{2}\Psi, \tag{4}$$

where $\Box = g^{cd}\nabla_c\nabla_d$, and as remarked above, we assume a potential describing a free but massive scalar field Ψ (hereafter boson field) with mass μ. We use geometrized units where $G = c = 1$.

Our task is to find solutions of the above system of field equations under several symmetries: we focus on stationary, axisymmetric, asymptotically flat (AF) spacetimes without "meridional currents," i.e., under the circularity condition. Therefore, we assume the existence of two Killing fields, ξ^a and η^a which are, respectively, timelike and spacelike, in the asymptotic regions, and are associated with the above symmetries. Due to the above assumptions, these Killing fields commute and therefore can be taken as a part of the coordinate basis. We use the time t and the spatial angle φ as coordinates adapted to such vector fields,

$$\xi^a = \left(\frac{\partial}{\partial t}\right)^a, \qquad \eta^a = \left(\frac{\partial}{\partial \varphi}\right)^a. \tag{5}$$

The circularity condition translates into $\xi^a R_a{}^{[b}\xi^c\eta^{d]} = \eta^a R_a{}^{[b}\xi^c\eta^{d]} = 0$ [30], which upon the use of the Einstein field Eq. (2), this condition imposes the following restrictions on the EMT: $\xi^a T_a{}^{[b}\xi^c\eta^{d]} = \eta^a T_a{}^{[b}\xi^c\eta^{d]} = 0$. In addition, the AF allows for the following conditions to be verified: $\xi_{[a}\eta_b\nabla_c\xi_{d]} = 0$, $\xi_{[a}\eta_b\nabla_c\eta_{d]} = 0$ on the (rotation) axis of symmetry [30]. These assumptions imply that the planes orthogonal to ξ_a and η_a are integrable (cf. Refs. [31–33]).

Thus far, we have local coordinates (t, x^1, x^2, φ), where the coordinates x^1, x^2 are associated with the two coordinate basis vectors $(\frac{\partial}{\partial x^1})^a$, $(\frac{\partial}{\partial x^2})^a$ respectively, which due to the previous hypothesis, are orthogonal to ξ^a and η^a, and thus, the metric components $g_{\mu\nu}$ with respect to the basis vectors satisfy $g_{t1} = g_{t2} = g_{\varphi 1} = g_{\varphi 2} = 0$, and the remaining no-null components are functions of x^1, x^2 solely. Furthermore, for the two coordinates x^1, x^2 we adopt the so-called Quasi-Isotropic gauge (QI) so that these coordinates are of spherical type r, θ and the metric reads[2]

$$ds^2 = -N^2dt^2 + A^2(dr^2 + r^2d\theta^2) + B^2r^2\sin^2\theta(d\varphi + \beta^{\varphi}dt)^2, \tag{6}$$

where the metric potentials N, A, B, β^{φ} are functions of the coordinates r, θ, solely. In particular, in the limit of spherical symmetry and staticity, the shift-vector component β^{φ} vanishes, and N, A, B become independent of the coordinate θ. Moreover, in that scenario $A(r) = B(r)$, and in vacuum such parametrization leads to the Schwarzschild solution in isotropic coordinates (cf. Appendix A).

QI coordinates (QIC) cover the DOC of the BH but they become singular at the horizon where the lapse function vanishes. Therefore in order for the differential equations to be valid at the horizon we impose suitable regularity conditions there (cf. Sec. II A). In practice QIC have proven to be very useful in analyzing several compact objects, in particular black hole spacetimes with scalar hair, mainly because the Einstein equations lead to a system of elliptic PDE for the metric potentials (or combinations of them) that can be solved numerically with great accuracy using spectral methods. Since in this paper we are not interested in solving the equations inside the BH, we do not require the use of more regular coordinates that cover its interior like Kruskal-Szekeres type of coordinates, which are usually adopted to obtain the maximal analytic extensions of some prominent exact BH solutions, as in the Schwarzschild and Kerr cases. Moreover, the ansatz (14) for the scalar field is consistent with the use of QIC.

That being said, other type of coordinates can be used as well. For instance, in a previous work configurations of black holes with scalar hair were obtained using maximal slicing and a spatial harmonic gauge [34]. Such coordinates are regular even on the horizon but they require the use of a more general ansatz for the scalar field.

Since the QI gauge for spacetimes with the above symmetries have been extensively used in the past [35,36], notably in the study of rotating boson stars [37], we proceed directly to write the specific Einstein equations for the metric potentials, which have been derived under the $3+1$ formalism of GR (for a review see [38–40]) and arranged in a more convenient fashion to take into account the spectral solver KADATH [28], and the fact that at the inner boundary, which represents the BH horizon $\mathcal{H}^{+}$, the lapse function N vanishes (cf. Sec. II A):

$$\Delta_3 N + \frac{\partial N\partial B}{B} - \frac{B^2r^2\sin^2\theta}{2}\frac{\partial\beta^{\varphi}\partial\beta^{\varphi}}{N} = 4\pi A^2 N(E+S), \tag{7}$$

$$\Delta_3(\beta^{\varphi}r\sin\theta) - \frac{\beta^{\varphi}}{r\sin\theta} - r\sin\theta\frac{\partial\beta^{\varphi}\partial N}{N} + 3r\sin\theta(\partial\beta^{\varphi}\partial\ln B) = 16\pi\frac{NA^2p_{\varphi}}{B^2r\sin\theta}, \tag{8}$$

[2]The reader is urged not to confuse the QI coordinates with the usual Boyer-Lindquist radial coordinates of Kerr geometry (cf. Appendix A).

$$N\Delta_2[(B-1)r\sin\theta]+[(B-1)r\sin\theta]\Delta_2 N + 2\partial N\partial[(B-1)r\sin\theta]+\Delta_2[(N-1)r\sin\theta] = 8\pi NA^2Br\sin\theta(S-S^{\varphi}_{\varphi}), \tag{9}$$

$$N\Delta_2 A + A\Delta_2 N - \frac{N}{A}\partial A\partial A - \frac{3}{4}AB^2r^2\sin^2\theta\frac{\partial\beta^{\varphi}\partial\beta^{\varphi}}{N} = 8\pi A^3 N S^{\varphi}_{\varphi}. \tag{10}$$

In this set of equations the following notation has been adopted:

$$\Delta_3 \equiv \frac{\partial^2}{\partial r^2}+\frac{2}{r}\frac{\partial}{\partial r}+\frac{1}{r^2}\frac{\partial^2}{\partial\theta^2}+\frac{1}{r^2\tan\theta}\frac{\partial}{\partial\theta}, \tag{11}$$

$$\Delta_2 \equiv \frac{\partial^2}{\partial r^2}+\frac{1}{r}\frac{\partial}{\partial r}+\frac{1}{r^2}\frac{\partial^2}{\partial\theta^2}, \tag{12}$$

and

$$\partial u\partial v \equiv \frac{\partial u}{\partial r}\frac{\partial v}{\partial r}+\frac{1}{r^2}\frac{\partial u}{\partial\theta}\frac{\partial v}{\partial\theta}. \tag{13}$$

As concerns the scalar field Ψ, we assume the following harmonic form on the time and angular dependence[3]:

$$\Psi(t,r,\theta,\varphi)=\phi(r,\theta)e^{i(\omega t-m\varphi)}, \tag{14}$$

where $\phi(r,\theta)$ is real valued and m is a nonzero integer. The harmonic dependence of the boson field is such that the EMT respects the symmetries of the underlying spacetime. As stressed in Ref. [41], and further analyzed in Ref. [20] the *noninheritance* of the spacetime symmetries in the scalar field via the harmonic time dependence and harmonic azimuthal angular dependence in (14) is crucial to obstruct the extensions of the existing no-hair theorems to the stationary and rotating scenarios where the EMT respects the symmetries of the underlying spacetime. The other ingredient that leads to bound (stationary) states for the scalar field is the synchronicity condition given below in Eq. (26) from which one notes that in the absence of both rotation ($\Omega_H=0$) and the harmonic dependence ($m=0$) the scalar field becomes real valued in a static and spherically symmetric spacetime where several no-hair theorems apply [3–5]. Further remarks along these symmetry considerations are addressed in Refs. [42].

[3]In order to match the notation of Ref. [37] one has to use $m=k$. Moreover, the integer m of this paper is not to be confused with the scalar-field mass of that reference. Finally, to compare with [20,21] one has to transform $\omega\to-\omega$, $m\to-m$, i.e., to change a global sign in the harmonic dependence of Ψ.

The Klein-Gordon Eq. (4) then reads

$$\Delta_3\phi+\frac{A^2}{N^2}(\omega+\beta^{\varphi}m)^2\phi-\frac{m^2\phi}{r^2\sin^2\theta}\left(\frac{A^2}{B^2}\right)+\frac{1}{N}\partial\phi\partial N+\partial\phi\partial\ln B=A^2\mu^2\phi. \tag{15}$$

The system of elliptic PDEs provided by Eqs. (7)–(10) is equivalent but different from the system used previously by HR [18] under a different coordinate gauge. The source terms that appear at the rhs of Eqs. (7)–(10) are provided by the $3+1$ decomposition of the EMT (3) [37–40][4]:

$$E=\left[\frac{(\omega+m\beta^{\varphi})^2}{N^2}+\frac{m^2}{B^2r^2\sin^2\theta}\right]\frac{\phi^2}{2}+\frac{1}{2A^2}\left[\left(\frac{\partial\phi}{\partial r}\right)^2+\frac{1}{r^2}\left(\frac{\partial\phi}{\partial\theta}\right)^2\right]+\frac{\mu^2\phi^2}{2}, \tag{16}$$

$$p_{\varphi}=\frac{m}{N}(\omega+m\beta^{\varphi})\phi^2, \tag{17}$$

$$S^{\varphi}_{\varphi}=\left[\frac{(\omega+m\beta^{\varphi})^2}{N^2}+\frac{m^2}{B^2r^2\sin^2\theta}\right]\frac{\phi^2}{2}-\frac{1}{2A^2}\left[\left(\frac{\partial\phi}{\partial r}\right)^2+\frac{1}{r^2}\left(\frac{\partial\phi}{\partial\theta}\right)^2\right]-\frac{1}{2}\mu^2\phi^2, \tag{18}$$

$$S=\left[3\frac{(\omega+m\beta^{\varphi})^2}{N^2}-\frac{m^2}{B^2r^2\sin^2\theta}\right]\frac{\phi^2}{2}-\frac{1}{2A^2}\left[\left(\frac{\partial\phi}{\partial r}\right)^2+\frac{1}{r^2}\left(\frac{\partial\phi}{\partial\theta}\right)^2\right]-\frac{3}{2}\mu^2\phi^2. \tag{19}$$

The above components of the EMT in $3+1$ form are compatible with the circularity condition, namely, the components $T_{t\theta}$, T_{tr}, $T_{\varphi\theta}$, $T_{\varphi r}$ vanish identically. Incidentally, the component $T_{r\theta}$, which does not vanish, is not necessary to solve the above system of equations. We performed some basic tests to check the consistency of this system, namely, we verified that in vacuum they satisfy the exact Kerr solution in QIC (cf. Appendix A), as opposed to the Kerr solution in Boyer-Lindquist (BL) coordinates. At this point it is important to emphasize that BL coordinates have been used to find solutions (with the Kerr background fixed) of cloud configurations for the boson field Ψ [17,18,20,21,43], which in turn allowed the use of separation of variables for the radial and angular dependence θ of the boson field leading to Teukolsky type of equations [44].

[4]We stress a difference (possibly due to a typo—a misplaced right bracket–) in a similar expression in Eq. (A14) of [37].

A. Boundary (regularity) conditions

In order to solve the system of elliptic PDE's, appropriate regularity conditions are implemented. We consider an inner boundary corresponding to the BH horizon $\mathcal{H}^+$, that we assume to have a spherical topology, and thus, it is located at $r = r_H$. Therefore, we impose regularity conditions at $r = r_H$ for each of the metric potentials N, A, B, and β^φ. According to Hawking's rigidity theorem [45], when physically reasonable conditions are satisfied (weak energy condition and matter obeying hyperbolic equations—in dynamic situations), the event horizon of a stationary BH coincide with a Killing horizon. These conditions are verified in the current scenario. This theorem is compatible with the circularity condition [32,33]. In the present case the null geodesic generators of the horizon have as tangent the *helical* Killing field

$$\chi^a = \xi^a + \Omega_H \eta^a, \tag{20}$$

in the region where its norm vanishes, like in the Kerr BH, where

$$\Omega_H = -\left.\frac{\xi_a \xi^a}{\xi_a \eta^a}\right|_{\mathcal{H}^+} = -\left.\frac{\eta_a \xi^a}{\eta_a \eta^a}\right|_{\mathcal{H}^+} = \text{const}, \tag{21}$$

is the *angular velocity* of the horizon [46]. In terms of the $3+1$ variables

$$\Omega_H = -\beta^\varphi(r_H, \theta) = \text{const}. \tag{22}$$

This is the condition imposed on the shift vector at r_H.

As mentioned above, the BH horizon is located at the place where $\chi^a \chi_a|_{\mathcal{H}^+} = 0$. In terms of the $3+1$ variables this corresponds at the place where the lapse function vanishes $N(r_H, \theta) = 0$. Additionally, the *ergosphere* is defined as the region where the Killing field ξ^a becomes spacelike. The ergosurface corresponds to the spacetime points where $\xi^a \xi_a = 0$; this is where the metric component $g_{tt} = 0$. Outside the ergosphere the Killing field ξ^a is *timelike*, where it is possible to find *static observers*, i.e. observers with 4-velocity u^a_S parallel to ξ^a. However, inside the ergosphere, those observers no longer exist, and must rotate with a component in the direction of the *rotational* Killing field η^a [see Eqs. (5)]. It is precisely within the ergosphere where the Penrose process of *energy extraction* can take place.

As concern the metric potentials A and B, we assume that the event horizon $\mathcal{H}^+$ coincides with an *apparent horizon*, and so these potentials have to satisfy the following condition (see Appendix B):

$$\left[\frac{\partial}{\partial r}\left(\frac{1}{A}\right) + \frac{1}{A}\left(\frac{2}{A}\frac{\partial A}{\partial r} + \frac{1}{B}\frac{\partial B}{\partial r} + \frac{2}{r}\right)\right]_{r_H} = 0. \tag{23}$$

In particular, we checked that the condition (23) is verified exactly for the Kerr metric in QIC. It may seem strange to use just one boundary condition for the two quantities A and B. However, by looking at Eqs. (9) and (10) one can see that they are degenerate, in the sense that the factor in front of the highest derivative (i.e. the $N\Delta_2$ operators) vanishes at the inner boundary. Such degenerate equations cannot be solved with any boundary conditions. In the case at hand, it appears that Eq. (9), on the horizon, becomes a regularity condition and is treated as such by the solver. Equation (23) is treated as being the boundary condition associated with Eq. (10).

As regards the boson field, we consider the so-called *synchronicity* or *no-flux* condition across the horizon to ensure the existence of "bound states" associated with a stationary boson field [17,18],

$$\chi^a \nabla_a \Psi|_{\mathcal{H}^+} = 0. \tag{24}$$

In view of Eq. (14), this condition translates into

$$(\omega - m\Omega_H)\Psi_H = 0. \tag{25}$$

So for any finite $\Psi_H \neq 0$ we obtain

$$\omega = m\Omega_H. \tag{26}$$

This condition stems also from demanding regularity in Eq. (15) at $\mathcal{H}^+$ as one can appreciate from the first term within brackets, which must vanish as the horizon is approached and where $N_H = 0$.

The Klein-Gordon equation (15) also requires some regularity condition to be fulfilled, due to the division by N. Close to the horizon the solver works with N times Eq. (15) to remove possible divergences. Doing so, the equation becomes degenerate [as for Eqs. (9) and (10)] and so it is solved without any boundary condition. This procedure allows to find the right value of the scalar field, consistent with regularity, without the need to enforce that regularity explicitly.

Asymptotic flatness (AF) is to be imposed on the spacetime, and thus, $\beta^\varphi \to 0$, $N \to 1$, $A \to 1$, $B \to 1$, as $r \to \infty$. Thanks to a compactification of space those conditions are enforced at exact infinity.

Now, when the background spacetime is fixed, one needs to solve only for the scalar field Eq. (15). With a Kerr background, the solution for Ψ leads to the cloud solutions mentioned before [17,18,20]. In this context, Eq. (15) is linear with respect to the scalar field and it admits nonzero solutions only for discrete values of the parameters (a, M, Ω_H, ω, and μ). So this is an eigenvalue problem. The numerical method thus needs some conditions to prevent the code from converging to the trivial solution $\phi(r, \theta) = 0$ and to find the right values of the parameters. A method for dealing with this class of problems (i.e. eigenvalue problems arising from a linear approximation) has already been used several times (see [47,48] and especially [34] in the

context of clouds). Using the same technique, clouds are constructed using a Kerr background in QI coordinates. They correspond to the limit of the full system when $\phi \to 0$. In this work, clouds are used as an initial guess to construct black holes with scalar hair, thus leading to the solution of the full nonlinear problem once we take into account the backreaction of the scalar field into the spacetime. By changing the parameters away from those of the cloud solutions, sequences of hairy BH can be obtained. For instance, in Fig. 6, the cloud solution corresponds to the rightmost point (with $\Omega_H/\mu \approx 0.98$) and the sequence is constructed by slowly varying Ω_H. We elaborate more about this point in Sec. IV.

As remarked before, the first test for the spectral code consisted of recovering numerically the exterior Kerr solution by setting the sources to zero, i.e., assuming a vacuum scenario with a vanishing scalar field. These tests are included in Appendix A, where we compare the numerical solution with the exact Kerr solution in QIC coordinates. The relative numerical errors are typically $\sim 10^{-14}$–10^{-16} or lower for 17 coefficients in the radial spectral expansion.

We perform a second test where we fix the Kerr background and recover the same kind of cloud solutions provided in Ref. [20] for the subextremal scenarios, but in QIC.

III. GLOBAL QUANTITIES, SURFACE GRAVITY AND BH THERMODYNAMICS

A. Boson number, mass and angular momentum

There are basically three global quantities that emerge as a consequence of the AF conditions which are measured at spatial infinity (as opposed to global quantities defined at $\mathcal{H}^+$). The first one is related to the internal symmetry associated with the boson field, namely, the invariance of the model with respect to a global phase transformation $\Psi \to \Psi' = e^{i\alpha}\Psi$, where $\alpha = \text{const}$. This symmetry leads to the local conservation of the *boson current* $\nabla_a j^a = 0$, where[5]

$$j^a = \frac{i}{2\hbar}(\Psi^* \nabla^a \Psi - \Psi \nabla^a \Psi^*). \tag{27}$$

Furthermore, the conserved current implies that the *total particle number* of the boson field is also conserved. This is given in terms of a volume integral on a spatial hypersurface Σ_t of the component of the flux j^a that is normal to the hypersurfaces Σ_t:

$$\mathcal{Q} \equiv \int_{\Sigma_t} -n_a j^a \sqrt{\gamma} d^3x, \tag{28}$$

where $\gamma = \det(\gamma_{ij}) = A^4 B^2 r^4 \sin^2\theta$ is the determinant of the three-dimensional metric, and $d^3x = dr d\theta d\varphi$. In this case the timelike normal is given by

$$n^a = \frac{1}{N}(\xi^a - \beta^\varphi \eta^a), \tag{29}$$

$$n_a = -N \nabla_a t = -N (dt)_a, \tag{30}$$

which is interpreted physically as the 4-velocity of observers that have *zero angular momentum* (ZAMO's) $\ell \equiv -n_a \eta^a \equiv 0$.

Using the harmonic form for the scalar field (14), the current (27) reduces to

$$j^a = \hbar^{-1} \phi^2 \nabla^a (m\varphi - \omega t), \tag{31}$$

and the total boson number is

$$\mathcal{Q} \equiv \frac{2\pi}{\hbar} \int_{r_H}^{\infty} \int_0^{\pi} \frac{1}{N}(\omega + m\beta^\varphi) \phi^2 A^2 B r^2 \sin\theta dr d\theta, \tag{32}$$

where we used the fact that all the quantities involved in the integral are independent of the angle φ due to the axial symmetry.

On the other hand, there are two global quantities at spatial infinity related to the spacetime symmetries. The first one is the *Komar mass*, which is associated with the Killing vector $\xi^a = (\partial/\partial t)^a$ [30]:

$$M_K \equiv -\frac{1}{8\pi} \oint_S \nabla^a \xi^b dS_{ab}. \tag{33}$$

Since in the current scenario the scalar field is present outside the BH, this integral can be split into two contributions [38], one at the inner boundary corresponding to the intersection $\mathcal{H}_t \equiv \Sigma_t \cap \mathcal{H}^+$, between the spatial hypersurfaces Σ_t defined by the parameter t associated with the timelike Killing field ξ^a [cf. Eq. (5)], and the event horizon $\mathcal{H}^+$. The second contribution corresponds to a volume integral within a 2-sphere $\mathcal{S}_\infty \subset \Sigma_t$ that extends to spatial infinity. In both cases dS_{ab} is the area-element 2-form normal to both boundaries. Thus, Eq. (33) reads

$$M_K = M^{\mathcal{H}_t} + M^{\Sigma_t}. \tag{34}$$

The mass $M^{\mathcal{H}_t}$ can be written using the $3+1$ variables [38][6]:

[5]Some differences on sign in the current depend on conventions. Here we agree with [17], but we use a different variable Ψ that introduces a factor $1/2$ (cf. the EMT). For all the numerical calculations we take units where $\hbar = 1$.

[6]In Ref. [38] the normal s^a is taken pointing inward the horizon $\mathcal{H}_t$, i.e., $s^a \to -s^a$, and therefore there is a global sign difference in Eqs. (35) and (43) as compared with the same equations of Ref. [38].

$$M^{\mathcal{H}_t} = -\frac{1}{8\pi}\oint_{\mathcal{H}_t} \nabla^a \xi^b dS^{\mathcal{H}_t}_{ab} = \frac{1}{4\pi}\oint_{\mathcal{H}_t} (D_a N - K_{ab}\beta^b) s^a \sqrt{q} d^2x, \quad (35)$$

where $D_a N = \gamma^b_a \nabla_b N$, $\gamma^b_a = \delta^b_a + n_a n^b$, $K_{ab} = -\gamma^c_a \gamma^d_b \nabla_c n_d$, $s^a = \sqrt{g^{rr}}(\partial/\partial r)^a$ is the *outward* normal to $\mathcal{H}_t$, $q = A^2 B^2 r^4 \sin^2\theta$, is the determinant of the two-dimensional metric induced on $r = \text{const}$ surfaces, and $d^2x = d\theta d\varphi$. More specifically, $s^a D_a N = \sqrt{g^{rr}}\partial_r N = \partial_r N/A$ and $K_{ab}\beta^b s^a = K_{r\varphi}\beta^\varphi/A$. Therefore[7]

$$M^{\mathcal{H}_t} = \frac{r_H^2}{2}\int_0^\pi (\partial_r N - K_{r\varphi}\beta^\varphi) B \sin\theta d\theta|_{r_H} = \frac{r_H^2}{2}\int_0^\pi \left(\partial_r N - B^2 r^2 \sin^2\theta \frac{\partial_r \beta^\varphi}{2N}\beta^\varphi\right) B \sin\theta d\theta|_{r_H}, \quad (36)$$

where we used $K_{r\varphi} = B^2 r^2 \sin^2\theta \frac{\partial_r \beta^\varphi}{2N}$.

The volume integral at spatial infinity associated with the contribution M^{Σ_t} can be expressed in terms of the EMT associated with the matter [30,38], in this case associated with the EMT of the boson field (3):

$$M^{\Sigma_t} = 2\int_{\Sigma_t}\left(T_{ab} n^a \xi^b - \frac{1}{2} T n_a \xi^a\right)\sqrt{\gamma} d^3x, \quad (37)$$

this mass can be obtained as well from the conserved current $\nabla_a(-T^{ab}\xi_b) = 0$, which is associated with the stationary condition.

For the problem at hand, $T_{ab} n^a \xi^b = N^{-1}(T_{tt} - T_{t\varphi}\beta^\varphi)$. The components of the EMT involved in the previous expressions and its trace T appearing in Eq. (37) can be obtained directly from (3), which yield

$$M^{\Sigma_t} = 2\pi\int_{r_H}^\infty\int_0^\pi \left[\frac{2\omega}{N}(\omega + m\beta^\varphi)\phi^2 - N\mu^2\phi^2\right] \times A^2 B r^2 \sin\theta dr d\theta. \quad (38)$$

For instance, in vacuum, $M^{\Sigma_t} \equiv 0$, and for Schwarzschild and Kerr spacetime in QIC $M^{\mathcal{H}_t} \equiv M$ (cf. Appendix A).

On the other hand, since the spacetime considered in our analysis is AF, one can obtain the total energy of the system from the mass ADM, which is given by a surface integral at infinity in the following form [38,40]:

$$M_{\rm ADM} \equiv \frac{1}{16\pi}\oint_{r\to\infty} [\bar{D}^b \gamma_{ab} - \bar{D}_a(f^{cd}\gamma_{cd})] s^a \sqrt{q} d^2x, \quad (39)$$

[7]In principle, this integral can be evaluated at $r \to \infty$ as well as at $r = r_H$ when matter is absent.

where f^{cd} is the flat 3-metric, γ_{ab} is the 3-metric and $\bar{D}_a$ denotes the covariant derivative associated with the metric f^{cd}. For the physical system that we study, it is found that

$$M_{\rm ADM} = \frac{1}{8\pi}\int_0^{2\pi}\int_0^\pi [\bar{D}^j \gamma_{rj} - \bar{D}_r(f^{kl}\gamma_{kl})] \times B r^2 \sin\theta d\theta d\varphi\Big|_{r\to\infty} = -\frac{1}{8}\int_0^\pi \left[\frac{\partial}{\partial r}(A^2 + B^2) + \frac{B^2 - A^2}{r}\right] B r^2 \sin\theta d\theta\Big|_{r\to\infty}. \quad (40)$$

When we consider the Kerr spacetime in QIC, as $r \to \infty$ the leading terms of the metric potentials are as follows (cf. Appendix A): $A^2 \sim 1$, $B^2 \sim 1$, $\frac{\partial A^2}{\partial r} \sim -\frac{2M}{r^2}$ and $\frac{\partial B^2}{\partial r} \sim -\frac{2M}{r^2}$, so from Eq. (40), it is found that $M_{\rm ADM} = M$. Due to the AF assumption, the Komar mass $M_{\rm K}$ given by Eq. (34) coincides with the ADM mass (39).

The second global quantity defined at spatial infinity which is associated with the axial Killing vector $\eta^a = (\partial/\partial\varphi)^a$, is the *Komar angular momentum*. This quantity is given by an integral similar to the Komar mass (33) but replacing $\xi^a = (\partial/\partial t)^a$ by $\eta^a = (\partial/\partial\varphi)^a$ and introducing a factor "$-\frac{1}{2}$" [30]:

$$J_{\rm K} \equiv \frac{1}{16\pi}\oint_{\mathcal{S}_\infty} \nabla^a \eta^b dS_{ab}. \quad (41)$$

Similarly, this expression can be split into two contributions [38]:

$$J_{\rm K} = J^{\mathcal{H}_t} + J^{\Sigma_t}, \quad (42)$$

where $J^{\mathcal{H}_t}$ is given by the following expression in terms of $3+1$ variables [38]:

$$J^{\mathcal{H}_t} = \frac{1}{8\pi}\oint_{\mathcal{H}_t} K_{ab} s^a \eta^b \sqrt{q} d^2x. \quad (43)$$

More explicitly,

$$J^{\mathcal{H}_t} = \frac{r_H^2}{4}\int_0^\pi K_{r\varphi} B \sin\theta d\theta\Big|_{r_H} = \frac{r_H^4}{8}\int_0^\pi \frac{\partial_r \beta^\varphi}{N} B^3 \sin^3\theta d\theta\Big|_{r_H}. \quad (44)$$

The contribution J^{Σ_t} can be written in terms of a volume integral from the conserved current $\nabla_a(T^{ab}\eta_b) = 0$:

$$J^{\Sigma_t} = -\int_{\Sigma_t} T_{ab} n^a \eta^b \sqrt{\gamma} d^3x. \quad (45)$$

In this case $T_{ab} n^a \eta^b = N^{-1}(T_{t\varphi} - \beta^\varphi T_{\varphi\varphi})$, and from (3), one obtains

$$J^{\Sigma_t} = 2\pi m \int_{r_H}^{\infty}\int_0^{\pi} \frac{1}{N}(\omega + m\beta^{\varphi})\phi^2 A^2 B r^2 \sin\theta dr d\theta. \quad (46)$$

From (46) and (32) note that

$$J^{\Sigma_t} = m\mathcal{Q}\hbar, \quad (47)$$

that is, J^{Σ_t} is an integer multiple of the boson number $\mathcal{Q}\hbar$, as it happens also in the rotating boson-star scenario [37,49].

An equivalent expression of the Komar angular momentum is (see e.g. Eq. (8.77) in Ref. [38])

$$J_\infty \equiv \frac{1}{8\pi}\oint_{S_\infty} K_{ab}\eta^a s^b dS, \quad (48)$$

where, as before, $\eta^a = (\partial/\partial\varphi)^a$ and $s^a = \sqrt{g^{rr}}(\partial/\partial r)^a$. For our current analysis, this becomes

$$\begin{aligned} J_\infty &= \frac{1}{8\pi}\int_0^{2\pi}\int_0^{\pi} K_{r\varphi}\eta^{\varphi} s^r r^2 \sin\theta d\theta d\varphi\Big|_{r\to\infty} \\ &= \frac{1}{8}\int_0^{\pi}\frac{\partial_r\beta^{\varphi}}{N} B^3 r^4 \sin^3\theta d\theta\Big|_{r\to\infty}. \end{aligned} \quad (49)$$

For instance, in Kerr spacetime in QIC, as $r\to\infty$ the leading terms of the metric potentials are as follows (cf. Appendix A): $N\sim 1$, $A\sim 1$, $B\sim 1$ and $\beta^{\varphi}\sim -2J/r^3$, in agreement with Eq. (49).

While $M_{\rm K} \equiv M_{\rm ADM}$ and $J_{\rm K} = J_\infty$ are identities that hold exactly, from the numerical point of view this is not necessarily the case as each quantity is computed differently. At the end of the next section we show that both pairs of quantities converge to the same value as the number of coefficients in the spectral decomposition increase. This is an important convergence test that allows us to determine the precision of the spectral code that has been used to solve the Einstein-Klein-Gordon (EKG) system.

B. Surface gravity

Following Ref. [30] the surface gravity κ of a stationary BH is given in terms of the Killing field (20) by

$$\kappa^2 = -\frac{1}{2}(\nabla^a\chi^b)(\nabla_a\chi_b)|_{\mathcal{H}^+}. \quad (50)$$

This expression leads to the following formulas for the surface gravity associated with a stationary, axisymmetric and circular spacetime containing a BH with metric (6) (see Appendix C for the details):

$$\begin{aligned} \kappa &= \left\{\frac{1}{A}\left[(\partial_r N)^2 + \frac{1}{r^2}(\partial_\theta N)^2\right]^{1/2}\right\}_{r_H} \\ &= \left\{\frac{1}{2AN}\left[(\partial_r N^2)^2 + \frac{1}{r^2}(\partial_\theta N^2)^2\right]^{1/2}\right\}_{r_H}. \end{aligned} \quad (51)$$

From (51) one can check that the surface gravity for Schwarzschild and Kerr spacetimes using QIC (cf. Appendix A) leads to the usual expressions [30] in terms of the mass M and the angular momentum $a = J/M$ (cf. Appendix C).

C. Mass and BH thermodynamics formula

According to Ref. [30], stationary, rotating, axisymmetric and AFBH's like the ones we are analyzing here satisfy the following Smarr relation (using the notation of this section):

$$M_K = M^{\Sigma_t} + \frac{1}{4\pi}\kappa\mathcal{A} + 2\Omega_H J^{\mathcal{H}_t}, \quad (52)$$

where $\mathcal{A}$ is the *area* of the horizon, which in terms of the QIC is given by

$$\begin{aligned} \mathcal{A} &= r_H^2\int_0^{2\pi}\int_0^{\pi} AB\sin\theta d\theta d\varphi\Big|_{r_H} \\ &= 2\pi r_H^2\int_0^{\pi} AB\sin\theta d\theta\Big|_{r_H}. \end{aligned} \quad (53)$$

Using Eq. (34) in Eq. (52), we can write the following formula at the horizon:

$$M^{\mathcal{H}_t} = \frac{1}{4\pi}\kappa\mathcal{A} + 2\Omega_H J^{\mathcal{H}_t}. \quad (54)$$

Formula (52), obtained first by Bardeen, Carter and Hawking [50], was instrumental to derive the *first law* of BH mechanics. In particular, in the absence of matter outside the BH, the formula reduces to the one provided by Smarr [51] which takes the same form as (54).

For instance, in the case of Schwarzschild and Kerr BH's (cf. Appendix A) Eq. (54) simply reduces to $M^{\mathcal{H}_t} = M$.

The temperature of the BH horizon is defined as $T_H = \kappa/(2\pi)$, whereas the entropy $S_H = \mathcal{A}/4$.

IV. NUMERICAL ANALYSIS

To solve the system of elliptic partial differential equations (7)–(10) together with the Klein-Gordon equation (15), we have used the KADATH library, which, as mentioned above, implements the spectral methods to solve this type of system. Furthermore, to solve the EKG system, we have included the regularity conditions for the metric potentials N, A, B, and β^{φ}, and for the amplitude of the scalar field $\phi(r,\theta)$ that were described in Sec. II A. In this work we focus only on solutions corresponding to $n = 0$ (i.e. where ϕ has no nodes) and $m = 1$.

Figure 1 shows the metric potentials N and A, while Fig. 2 depicts B and β^{φ}, both for black hole solutions with scalar hair by fixing the coordinate at the horizon as $r_H = 0.057648/\mu$ and taking three different values of Ω_H.

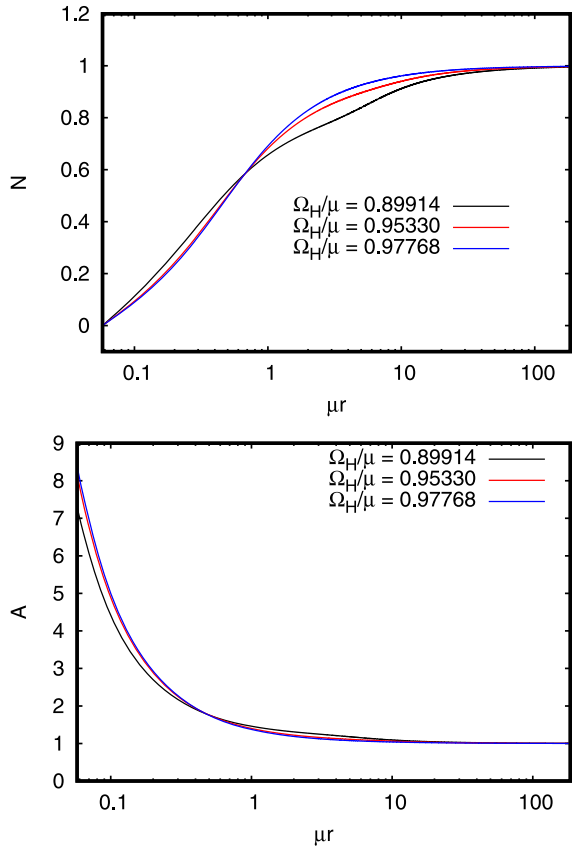

FIG. 1. Solutions for the lapse N and the metric function A (evaluated at the equator $\theta = \pi/2$) associated with the elliptic system Eqs. (7)–(10), with $\mu r_H = 0.057648$ and three different values of Ω_H.

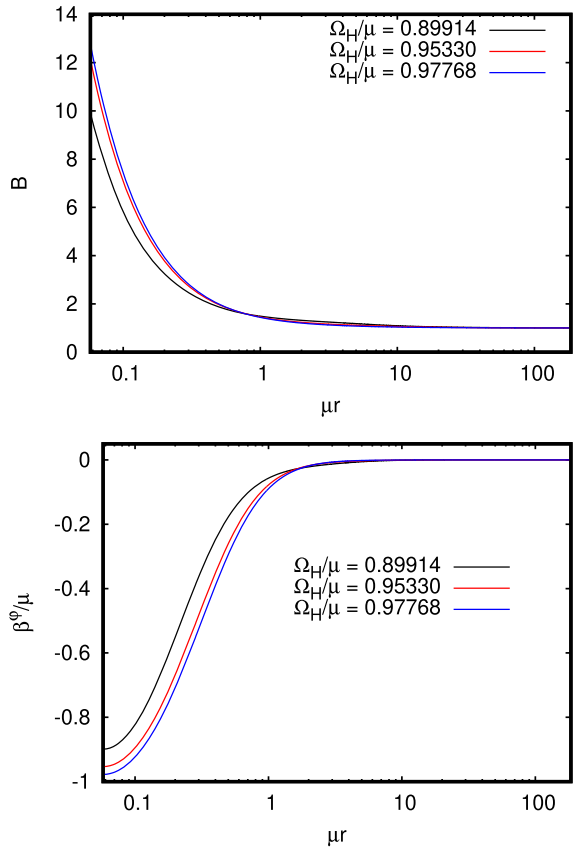

FIG. 2. Solutions for the function B and the shift β^φ (evaluated at the equator $\theta = \pi/2$) associated with the elliptic system Eqs. (7)–(10) with $\mu r_H = 0.057648$ and three different values of Ω_H.

Figure 3 shows the corresponding solutions for the scalar-field amplitude $\phi(r, \theta)$ at the equatorial plane ($\theta = \pi/2$). The values of ϕ together with the corresponding metric potentials shown in Figs. 1 and 2 are examples of solutions of the full EKG system, and as such, they represent black hole solutions endowed with scalar hair.

We stress that these solutions are regular in the DOC, notably, at the event horizon. Moreover, we appreciate that asymptotically the scalar field vanishes and the metric functions match the Minkowski values ($N \to 1$, $A \to 1$, $B \to 1$, and $\beta^\varphi \to 0$).

Figure 4 shows the scalar field near the horizon ($r_H \approx 0.058/\mu$) in order to appreciate closely the regularity conditions there. Figure 5 displays a family of scalar-field solutions ϕ at the equatorial plane taking different values for r_H and Ω_H.

Figure 6 depicts the Komar mass (33) and the Komar angular momentum (41) for a sequence of hairy black hole solutions with different values of Ω_H, but keeping fixed the horizon at $r_H = 0.057648/\mu$. Note that these global quantities are very sensitive to small variations of the angular velocity of the black hole. The larger the angular velocity, the lower the amplitude of the scalar-field results (cf. Fig. 3), and therefore the Komar quantities become smaller as the scalar-field contribution decreases in the DOC.

As a measure of the contribution of the scalar field Ψ to the black hole solution, it is convenient to define the

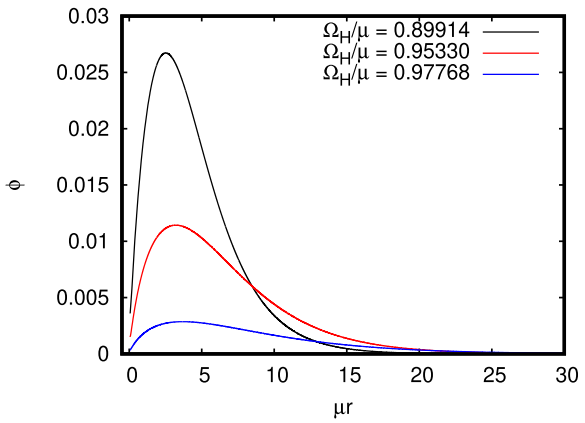

FIG. 3. Scalar-field solutions $\phi(r, \pi/2)$ for a black hole with $\mu r_H = 0.057648$ and three different values of Ω_H.

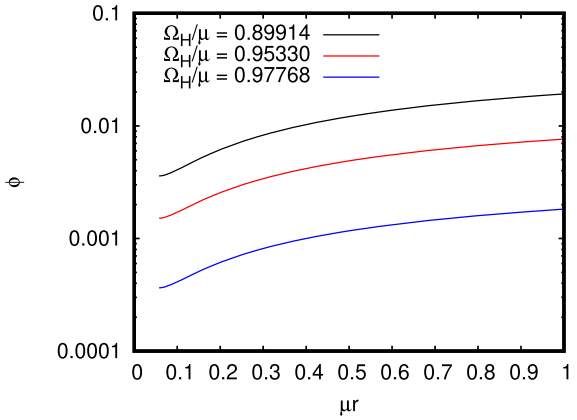

FIG. 4. Scalar-field solutions $\phi(r, \pi/2)$ associated with Fig. 3, but depicted close to the horizon located at $\mu r_H = 0.057648$.

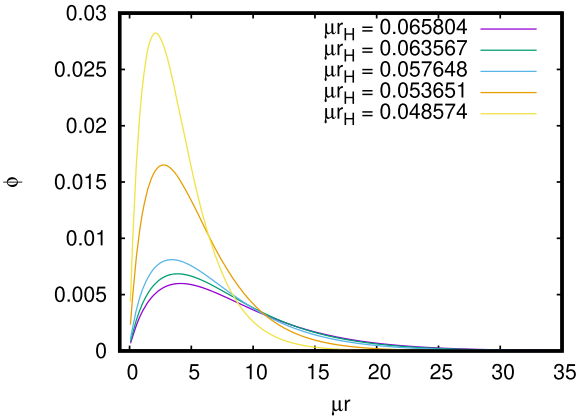

FIG. 5. Scalar-field solution $\phi(r, \pi/2)$ for different values of r_H and Ω_H (the latter are not shown).

dimensionless quantity q, in terms of the Noether charge $\mathcal{Q}$ and the total angular momentum J_{K}, as follows:

$$q \equiv \frac{m\mathcal{Q}}{J_{\mathrm{K}}}. \tag{55}$$

From the expressions given by Eqs. (44) and (45) it is easy to see that for a Kerr black hole $q = 0$, since in this scenario the Noether charge vanishes identically, while for a boson star (no horizon is present) $q = 1$ because in this case $J_{\mathrm{K}} = J^{\Sigma_t}$ and $J^{\Sigma_t} = m\mathcal{Q}$ (i.e. $M^{\mathcal{H}_t} = 0 = J^{\mathcal{H}_t}$). By continuity we may conclude that the quantity q takes values in the interval (0, 1) when we consider a black hole solution with scalar hair.

Figure 7 depicts the quantity q as a function of Ω_H for two different sequences of solutions of the Einstein-Klein-Gordon system corresponding to hairy black holes with event horizons fixed at $r_H = 0.057648/\mu$ (top panel) and $r_H = 0.053651/\mu$ (bottom panel). In both plots we observe how the quantity q approaches 1 as the angular velocity of the black hole with scalar hair moves away from the value of Ω_H corresponding to a Kerr black hole from which the

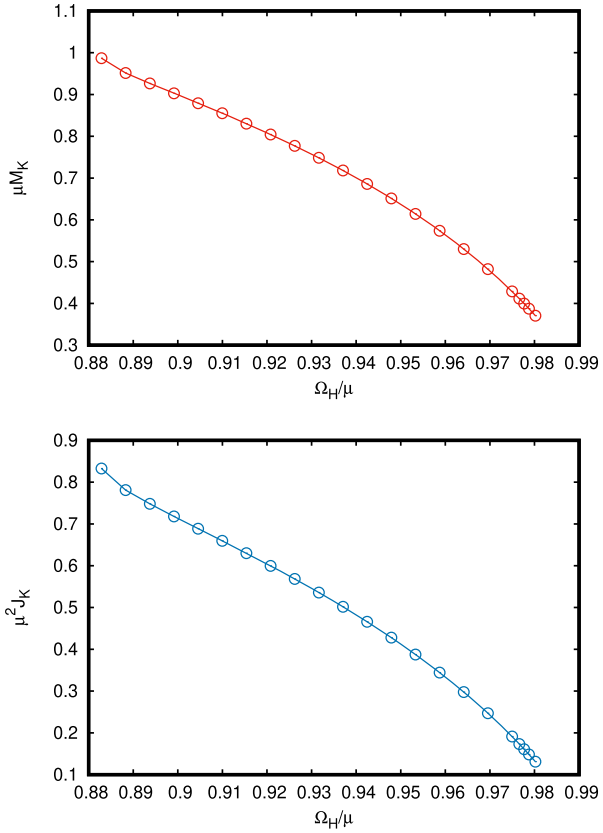

FIG. 6. Komar mass (top panel) and Komar angular momentum (bottom panel) as a function of Ω_H for hairy BH solutions with $\mu r_H = 0.057648$ fixed.

sequence of solutions were generated. This result is a consequence of the fact that the value of the amplitude of the scalar field ϕ increases as Ω_H decreases from the initial guess configuration.

Figure 8 shows the contribution of the black hole mass at the horizon, $M^{\mathcal{H}_t}/M_{\mathrm{ADM}}$, and the corresponding contribution of the scalar-field mass $M^{\Sigma_t}/M_{\mathrm{ADM}}$, relative to the total mass, for the family of hairy black holes associated with the values $\mu r_H = 0.057648$ and $\mu r_H = 0.053651$, respectively, as a function of Ω_H. When the former contribution is lower, the latter is larger and vice versa because both fractions add to one according to Eq. (34), where $M_{\mathrm{K}} \equiv M_{\mathrm{ADM}}$.

Figure 9 depicts the dimensionless quantity $J_\infty/M^2_{\mathrm{ADM}}$ as a function of Ω_H for three different sequences of hairy black holes associated with the event horizons located at $\mu r_H = 0.057648$, $\mu r_H = 0.053651$ and $\mu r_H = 0.048574$, respectively. We appreciate that this quantity is not bounded from above by unity, unlike the Kerr black hole where $0 \leq |a/M| \leq 1$ ($a = J/M$ and $M_{\mathrm{ADM}} = M$ for Kerr) (cf. tables in Appendix E). This behavior is an indicator of how different the hairy configurations can be relative to the vacuum Kerr solution.

Figure 10 shows the surface gravity κ (see Appendix C) for the same sequence of solutions that appear in Fig. 9.

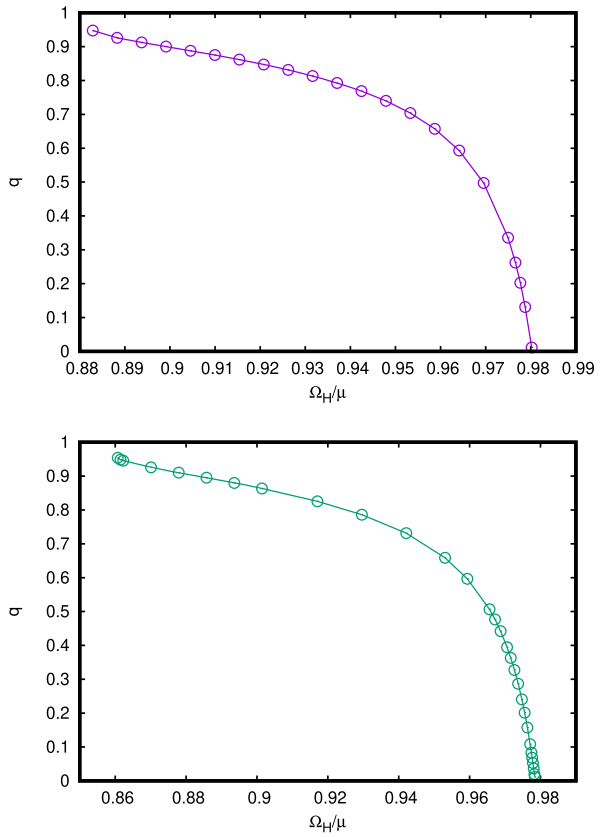

FIG. 7. The dimensionless quantity $q = m\mathcal{Q}/J_{\rm K}$ as a function of Ω_H for hairy black holes with event horizon at $\mu r_H = 0.057648$ (top panel) and $\mu r_H = 0.053651$ (bottom panel), respectively.

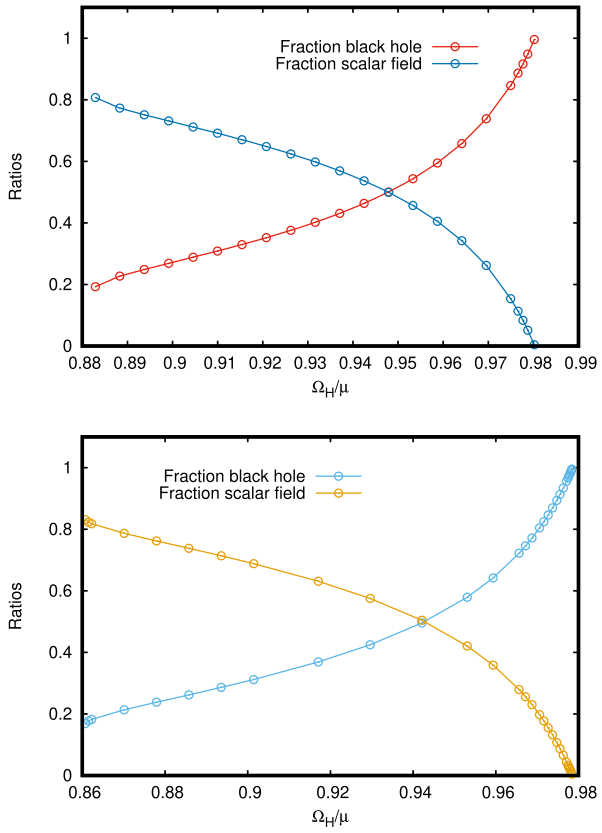

FIG. 8. Relative mass contributions $M^{\mathcal{H}_t}/M_{\rm ADM}$ and $M^{\Sigma_t}/M_{\rm ADM}$ as a function of Ω_H. In these plots the event horizon is located at $\mu r_H = 0.057648$ (top panel) and $\mu r_H = 0.053651$ (bottom panel), respectively.

Figure 11 plots the metric component $g_{tt} = -N^2 + B^2(\beta^\varphi)^2 r^2 \sin^2\theta$ as a function of the coordinate r (on the equatorial plane), in order to locate the ergosurfaces associated with the regions where $g_{tt} = 0$. Here we have considered three hairy black holes with fixed $\mu r_H = 0.057648$ but for three different values of the angular velocity Ω_H, as shown in the figure.

Figure 12 depicts the existence lines (diagram $M_{\rm ADM}$ vs ω) associated with the hairy black hole solutions when solving the full EKG system for a fixed r_H (we consider six different sequences) and varying the value Ω_H. The values of r_H are shown in the figure for each sequence of solutions, and as stressed before, all of them correspond to the integers $n = 0$ and $m = 1$. The blue solid line corresponds to the (vacuum) extremal Kerr solution $|a| = M$, while the magenta solid line represents configurations associated with boson stars with $m = 1$. The latter were computed with the spectral code used in Ref. [37]. The black dashed line corresponds to the scalar cloud solutions in a Kerr spacetime in QI coordinates with $n = 0$ and $m = l = 1$ (see Appendix D).

Figure 13 shows the existence lines in a diagram $M_{\rm ADM}$ vs J_∞ for the same sequence of solutions that appear in Fig. 12.

In Fig. 14 we compare the ADM mass (39) with the value obtained using Eq. (52), which involves thermodynamic quantities associated with the BH's event horizon. This is for a sequence of hairy black holes with $\mu r_H = 0.057648$ and different values of Ω_H. The relative error between both quantities is $\sim 10^{-6}$. Table X displays several values of the

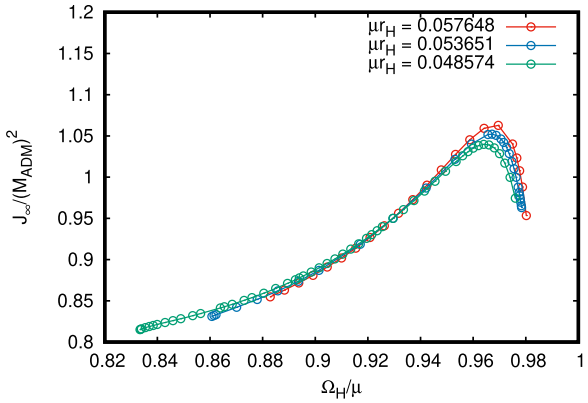

FIG. 9. The dimensionless parameter $J_\infty/M^2_{\rm ADM}$ as a function of Ω_H for hairy black holes with three different horizon values.

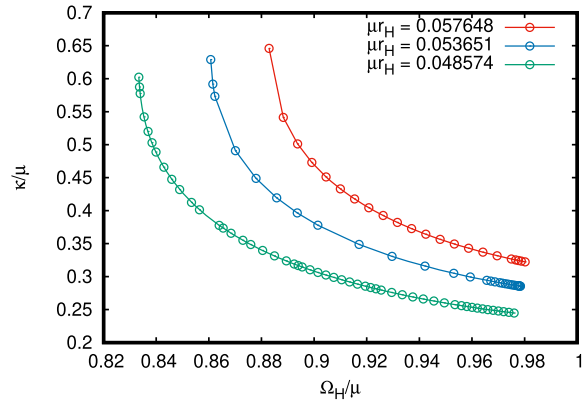

FIG. 10. Surface gravity κ as a function of Ω_H for hairy BH's with three different horizon values.

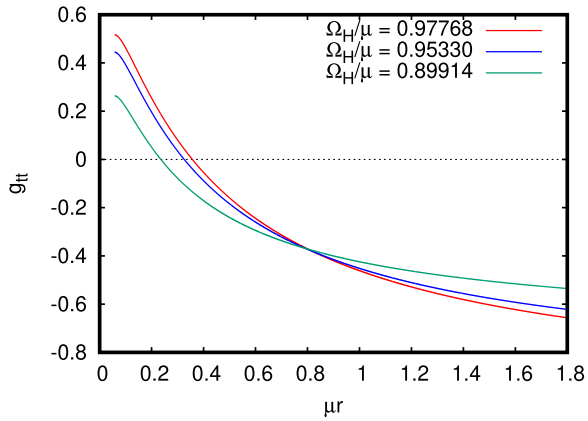

FIG. 11. Localization of ergosurfaces on the equatorial plane ($\theta = \pi/2$) for three hairy black hole with fixed $\mu r_H = 0.057648$.

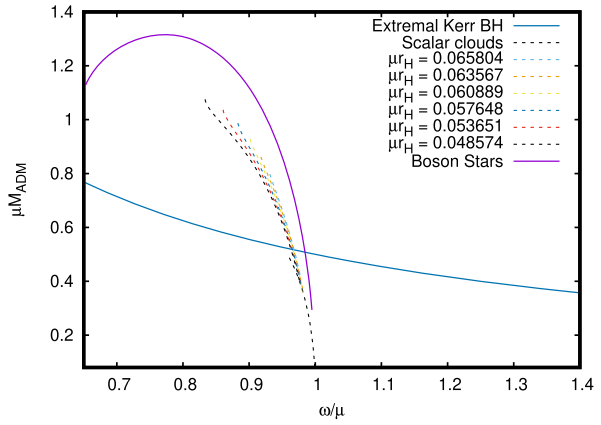

FIG. 12. Existence lines for hairy black holes—colored dashed lines—(diagram $M_{\rm ADM}$ vs ω). Each sequence has a fixed r_H, and six sequences are computed. The solid (magenta) line is associated with rotating boson stars, while the (blue) solid line corresponds to extremal Kerr BH's ($M = 1/2\Omega_H$). The (black) dashed line that starts close to the values $\mu M = 0.1$, $\omega/\mu = 1$ and ends close to the extremal (blue) solid line is the existence line for *boson clouds* in the background of Kerr BH's. Here $\omega = \Omega_H$ ($m = 1$) for the hairy solutions and the boson clouds.

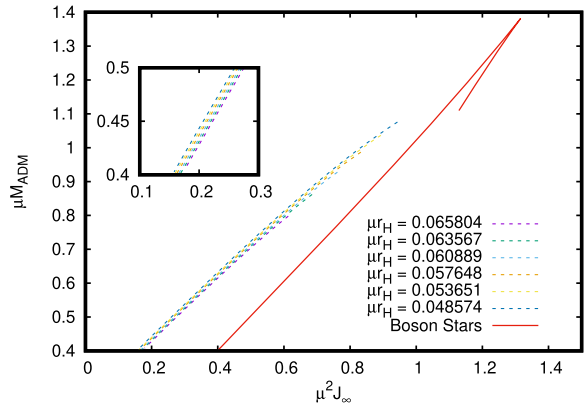

FIG. 13. Existence lines for hairy black holes in a diagram $M_{\rm ADM}$ vs J_∞.

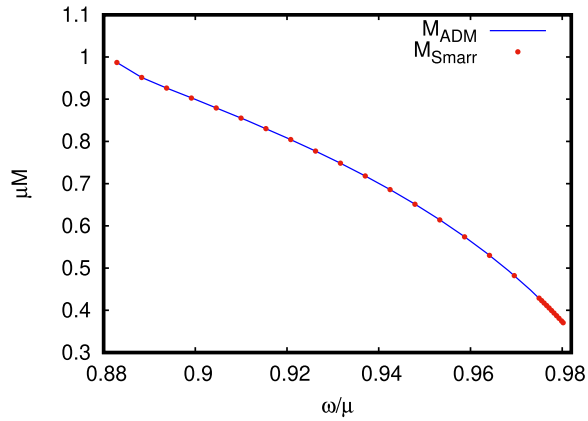

FIG. 14. Comparison between the ADM mass and the (Smarr) mass obtained from Eq. (52) for hair BH's with fixed $\mu r_H = 0.057648$.

thermodynamic quantities $\{T_H, \mathcal{A}, S_H\}$ associated with the hairy BH's.

Figures 15 and 16 show the error indicators for different spectral resolutions of hairy BH solutions characterized by two different values of r_H and Ω_H. The top panel of each figure corresponds to the relative difference between the ADM mass and the Komar mass defined as $|M_{\rm K} - M_{\rm ADM}|/|M_{\rm K} + M_{\rm ADM}|$, while the bottom panel corresponds to the relative difference between expressions (48) and (41) for the angular momentum defined as $|J_{\rm K} - J_\infty|/|J_{\rm K} + J_\infty|$. Another error indicator, depicted in Fig. 17, is the relative difference between the two expressions for the Komar mass $M_{\rm K}$, given by Eqs. (33) and (34), where in practice (33) is computed using the expression (36) but instead of evaluating at r_H it is computed at $r \to \infty$. The error indicators display the characteristic exponential convergence with the expansion number of radial coefficients in the spectral decomposition [27].

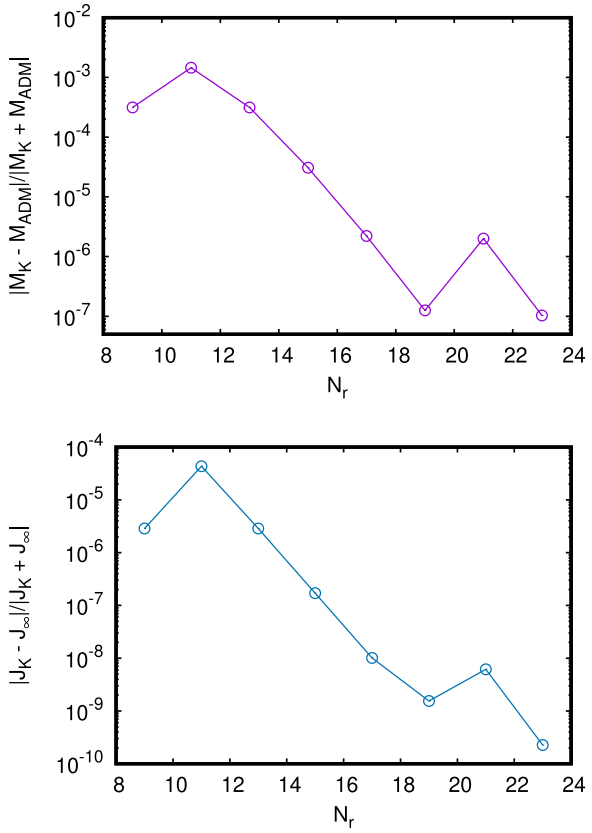

FIG. 15. Error indicators between the Komar and ADM masses and between expressions (42) (J_K) and (48) (J_∞) of the total angular momentum associated with a hairy black hole with event horizon at $\mu r_H = 0.057648$ and angular velocity $\Omega_H/\mu = 0.88289$, as a function of the number of radial coefficients in the spectral expansion.

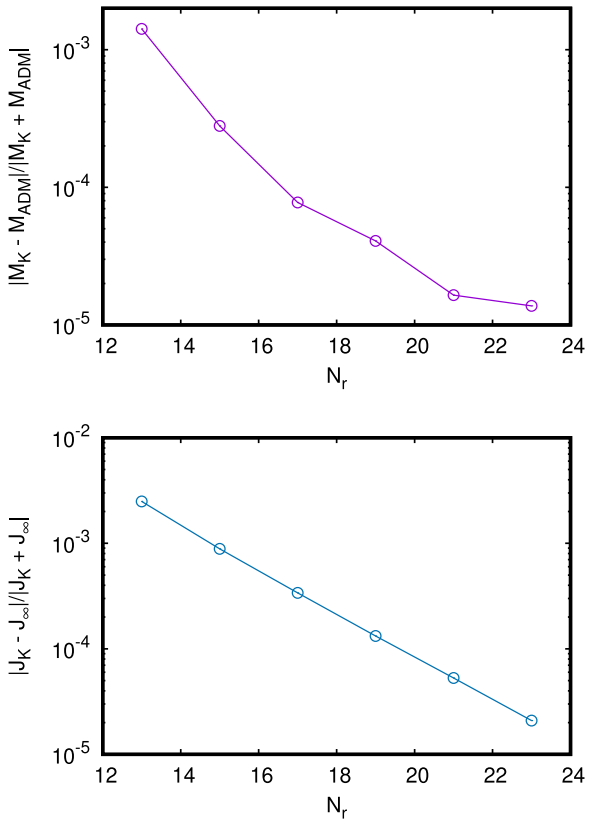

FIG. 16. Similar to Fig. 15 with $\mu r_H = 0.048574$ and angular velocity $\Omega_H/\mu = 0.97594$.

V. COMPARISON WITH PREVIOUS STUDIES

The cloud solutions in a fixed Kerr background (in QIC) are used as initial guess to compute the full hairy solutions. Thus, we recovered first the same kind of clouds found earlier by Herdeiro and Radu [17] and also in Ref. [20], where BL coordinates were employed instead. Some examples of these cloud configurations are depicted in Appendix D. In contrast, Herdeiro and Radu departed from a boson star configuration (i.e. a globally regular scalar-field solution without a horizon) as "initial guess" for the scalar field, and from that configuration they computed the rotating hairy BH's (RHBH) solutions.

Following the above strategy we obtained RHBH solutions similar to those reported in Refs. [17,18]. The space of solutions can be summarized in the *existence lines* depicted as plots $M_{\rm ADM}$ vs ω (cf. Fig. 12) which are similar to Figs. 4 and 6 of Ref. [18].

A more direct and quantitative comparison between our results and those of Ref. [18] is difficult due to the use of different coordinates and parametrization of the metric. The main contrast between both analyses, ours and theirs, is that for the moment we cannot recover the globally regular boson star configurations directly from our spectral code since our parametrization for the metric and the implementation of the boundary conditions do not allow us to take the limit $r_H \to 0$ corresponding to a regular origin. In the present parametrization, this limit is (in principle) associated with an extremal RHBH. This can be better appreciated in the Kerr (vacuum) scenario from Eq. (A8) where the horizon for an extremal Kerr BH in BL coordinates is located at $R = M$, which corresponds to $r_H = 0$ in the QI coordinates. We plan to overcome these limitations in the future, which in addition will allow us to study the exact extremal hairy configurations with exactly vanishing surface gravity κ, and not only in the limit of small values. Some of these values of κ can be appreciated from the last rows of Tables VIII and IX associated with a RHBH that is close to an extremal Kerr due to a small contribution of the scalar hair to the total mass (cf. columns 5 and 7 of those tables). As we discussed already, the solid (magenta) line of Fig. 12 corresponding to boson stars was obtained from an independent and different, albeit similar, spectral code used in Ref. [37]. There, rotating boson star models have been computed with regularity conditions imposed at the origin, as opposed to the regularity conditions at the horizon imposed here. Due to the limitations alluded to before we appreciate from Fig. 12 that the

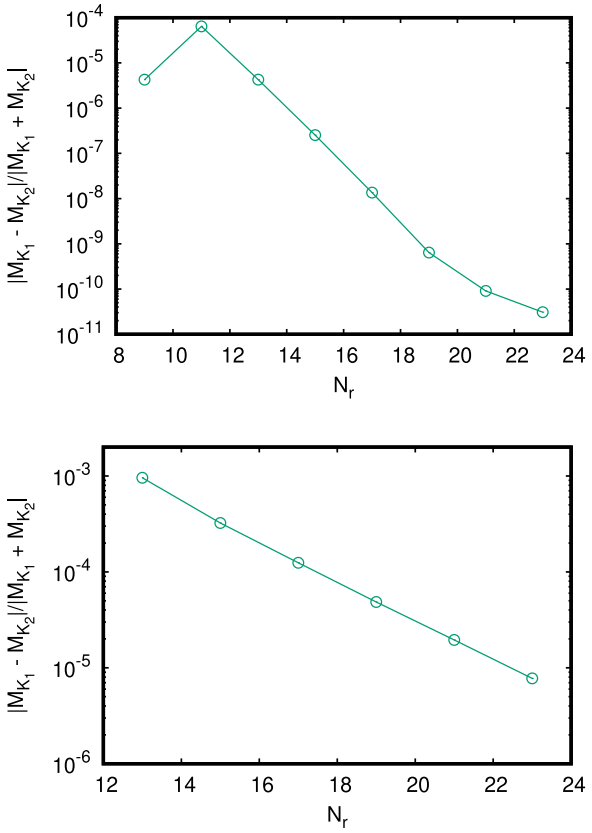

FIG. 17. Error indicators associated with the Komar mass M_{K} when using the two expressions given by (33) and (34), labeled as M_{K_1} and M_{K_2} in the figure, respectively. The top panel correspond to $\mu r_H = 0.057648$ and angular velocity $\Omega_H/\mu = 0.88289$, and the bottom panel to $\mu r_H = 0.048574$ and $\Omega_H/\mu = 0.97594$.

existence (dashed) lines of HRBH do not connect continuously to the boson star (magenta) solid line, but finish in a configuration with $q < 1$. The existence lines do not have a constant q, but a constant r_H; therefore, our lines "cross along" the corresponding (dashed) curves of Fig. 4 of Ref. [18] which are depicted for $q = \text{const}$.

Moreover, as in Ref. [18], we find that the dimensionless parameter $J_\infty/M^2_{\mathrm{ADM}}$ can be larger than unity in RHBH unlike the (hairless) Kerr BH's where $0 \leq |J/M^2| \leq 1$ (see the last columns of Tables IV–IX).

In the full nonlinear treatment as well as in the cloud (linear) study—where the Kerr background is fixed—the scalar-field solution vanishes identically if the rotation is "turned off" (e.g. taking $m = 0$), which is consistent with the no-hair theorem in spherical symmetry [4,5].[8] This is something that was also remarked in Ref. [18].

[8]In this case, due to the synchronicity condition (26), when $m = 0$ automatically $\omega = 0$ and the scalar field becomes real valued.

VI. CONCLUSIONS AND OUTLOOK

We have confirmed that rotating black holes can support hair under the form of a complex-valued scalar field using a completely independent code and a numerical method different from Ref. [18]; namely, we used QI coordinates and spectral methods. We have provided different numerical tests (convergence tests and comparison with the Kerr exact solution in vacuum) that indicate the robustness of our numerical analysis. The existence of a nontrivial configuration of this scalar field avoids the no-hair theorems due to the rotation of the black hole (see Refs. [20,21] for a deeper discussion). We have computed plenty of hairy configurations, including the computation of several global quantities (see Appendix E), showing that the hair can contribute substantially to the total (ADM or Komar) mass of the BH. This indicates that the hairy solutions can differ drastically from the Kerr solution. However, for configurations having a "diluted" hair, the solutions are similar to the cloud solutions (see Appendix D) where the scalar field can coexist in the background of a Kerr BH. A particular feature of the hairy solutions is that the dimensionless parameter $J_\infty/M^2_{\mathrm{ADM}}$ can take values $|J_\infty/M^2_{\mathrm{ADM}}| > 1$, even when solutions are relatively "far" from *extremality* (e.g. the surface gravity $\kappa \sim 0.5\mu$) unlike the Kerr solution where $|a/M| \leq 1$, and the upper bound is reached in the extremal case $a = M$ where $\kappa = 0$. As argued in Ref. [18] this is because hairy configurations can connect continuously to the solitonic (rotating boson star) solutions where that dimensionless quantity can also exceed unity.

As we mentioned in the Introduction, from the observational point of view it is perhaps too early to appreciate the impact of these hairy solutions for different reasons. So far, all direct detection of dark matter particles has failed. Thus, it is still unclear if a fundamental complex-valued scalar field could be associated with dark matter or not. On the other hand, it is also unclear if the dark matter phenomenology could be instead explained by an alternative theory of gravity, since all the proposals in that direction have also failed to recover in addition all the success of GR. Notwithstanding, we have at our disposal several instruments that can validate, bound or rule out the existence of this kind of hairy solution in a near future. For instance, since these solutions produce a spacetime different from the Kerr solution, their respective *shadows* can be different since the photon trajectories are affected differently (cf. Refs. [52]). Moreover, the gravitational waves emitted from the collision of two RHBH can have a different pattern relative to the Kerr counterparts, and so the LIGO-VIRGO observatories, as well as the forthcoming detectors KAGRA, Einstein Telescope and LISA can put stringent bounds to such solutions or perhaps indicate deviations from the standard Kerr BH interpretation that might be explained by the RHBH. These are scenarios that are worth of study. Moreover, it has been argued [53] that RHBH could be constrained by the analysis of the expected x-ray

spectra produced by accretion disks around BH's with the forthcoming x-ray missions, like Suzaku, eXTP and LOFT [54]. Finally, recently an *unusual* gravitational wave detection GW200129 by the LIRGO-VIRGO collaboration triggered speculations about possible deviations from GR, so that BH's from alternative theories could explain such "anomalous" signals (cf. [55]). Nevertheless, a recent analysis [56] presents strong evidence showing that such signals are due to the collision of two "ordinary" Kerr BH's that, however, precess violently and together with the tilt and the high spin of the primary BH with respect to the orbital angular momentum, can explain the unusual gravitational wave patterns. This example teaches us that the answer to an unexpected phenomenon can be found within GR before jumping to much more exotic explanations. Thus, hairy BH's within GR itself can be a potential candidate to explain some unexpected features that might be revealed in the forthcoming observations related with BH astrophysics without the need to resort to much more drastic avenues like modified theories of gravity. Therefore, it is worth exploring different properties (e.g. stability [22,23] and extremality) and variations around this kind of RHBH solution.

ACKNOWLEDGMENTS

This work was supported partially by DGAPA–UNAM Grants No. IN111719, No. IN105223, and CONACYT (FORDECYT-PRONACES) Grant No. 140630. G. G. acknowledges CONACYT Scholarship No. 291036. G. G. and M. S. are indebted to E. Murrieta and L. Díaz for their help in installing and parallelizing the spectral code at the ICN cluster. E. G. and P. G. acknowledge funding by l'Agence Nationale de la Recherche, Project No. StronG ANR-22-CE31-0015-01.

APPENDIX A: KERR METRIC IN QUASI-ISOTROPIC COORDINATES AND NUMERICAL TESTS

Before providing the Kerr solution in QIC we present the Kerr solution in Boyer-Lindquist coordinates (BLC), (t, R, θ, φ), in order to contrast both solutions[9]:

$$ds^2 = -\frac{(\Delta - a^2\sin^2\theta)}{\Sigma}dt^2 - \frac{2a\sin^2\theta(R^2+a^2-\Delta)}{\Sigma}dtd\varphi + \frac{\left[(R^2+a^2)^2 - \Delta a^2\sin^2\theta\right]}{\Sigma}\sin^2\theta d\varphi^2 + \frac{\Sigma}{\Delta}dr^2 + \Sigma d\theta^2, \tag{A1}$$

where

$$\Sigma = R^2 + a^2\cos^2\theta, \tag{A2}$$

$$\Delta = R^2 + a^2 - 2MR = (R - R_+)(R - R_-), \tag{A3}$$

and

$$R_+ = M + \sqrt{M^2 - a^2}, \tag{A4}$$

$$R_- = M - \sqrt{M^2 - a^2}. \tag{A5}$$

The event horizon is located at $R_H = R_+$.
The lapse function is given by

$$N^2 = \frac{\Delta\Sigma}{(R^2+a^2)^2 - \Delta a^2\sin^2\theta}. \tag{A6}$$

The relationship between the BLC (t, R, θ, φ) and the QIC (t, r, θ, φ) is as follows [36]:

$$R = r + M + \frac{M^2 - a^2}{4r}, \tag{A7}$$

$$r = \frac{1}{2}\left(R - M + \sqrt{\Delta}\right) = \frac{1}{2}\left(R - M + \sqrt{R^2 - 2MR + a^2}\right). \tag{A8}$$

$$A^2 = \frac{-2a^2M(M+4r) + 8a^2r^2\cos(2\theta) + a^4 + (M+2r)^4}{16r^4}, \tag{A9}$$

$$N^2 = 16r^4\left(1 - \frac{\sqrt{M^2-a^2}}{2r}\right)^2\left(1 + \frac{\sqrt{M^2-a^2}}{2r}\right)^2[-2a^2M(M+4r) + 8a^2r^2\cos(2\theta) + a^4 + (M+2r)^4] \times [8a^2r^2\cos(2\theta)(a^2 - M^2 + 4r^2)^2 - 4a^6(M^2 + 4Mr - 2r^2) - 4a^2(M+2r)^2(18M^2r^2 + 8M^3r + M^4 - 8Mr^3 - 8r^4) + a^8 + (M+2r)^8 + a^4(96M^2r^2 + 48M^3r + 6M^4 - 64Mr^3 + 32r^4)]^{-1}, \tag{A10}$$

[9]We use the notation R for the radial BLC, since r is reserved here for the QIC.

$$B^2 = [8a^2r^2\cos(2\theta)(a^2 - M^2 + 4r^2)^2 - 4a^6(M^2 + 4Mr - 2r^2) + a^4(96M^2r^2 + 48M^3r + 6M^4 - 64Mr^3 + 32r^4)$$
$$- 4a^2(M + 2r)^2(18M^2r^2 + 8M^3r + M^4 - 8Mr^3 - 8r^4) + a^8 + (M + 2r)^8]$$
$$\times [16r^4(-2a^2M(M + 4r) + 8a^2r^2\cos(2\theta) + a^4 + (M + 2r)^4)]^{-1}, \tag{A11}$$

and

$$\beta^\varphi = [128aMr^3(a - M - 2r)(a + M + 2r)] \times [8a^2r^2\cos(2\theta)(a^2 - M^2 + 4r^2)^2$$
$$- 4a^6(M^2 + 4Mr - 2r^2) + a^4(96M^2r^2 + 48M^3r + 6M^4 - 64Mr^3 + 32r^4)$$
$$- 4a^2(M + 2r)^2(18M^2r^2 + 8M^3r + M^4 - 8Mr^3 - 8r^4) + a^8 + (M + 2r)^8]^{-1}. \tag{A12}$$

We have checked using *SageMath* that the above values of A, B, N and β^φ define a metric that fulfills the vacuum $3+1$-Einstein equations.[10] We have also checked using *Mathematica* that they satisfy the elliptic equations (7)–(10) in the absence of matter. Moreover, in the nonrotating limit $a = 0$, the above variables reduce to the usual expressions for the Schwarzschild metric in isotropic coordinates with $A = B$, $\beta^\varphi = 0$, and

$$N = \frac{1 - \frac{M}{2r}}{1 + \frac{M}{2r}}, \tag{A13}$$

$$A = \left(1 + \frac{M}{2r}\right)^2. \tag{A14}$$

Figures 18 and 19 depict the numerical and the exact solutions for Kerr spacetime. Figures 20 and 21 show the corresponding relative errors between those solutions.

APPENDIX B: APPARENT HORIZON

We follow the approach of Refs. [39,40] and consider a smooth, closed, two-dimensional (spatial) surface $\mathcal{S}$ embedded in Σ_t, and take s^a as its outward-pointing unit normal tangent to Σ_t satisfying $s^a s_a = 1$ and $s^a n_a = 0$. The two-dimensional metric m_{ab} on $\mathcal{S}$ induced by γ_{ab} is

$$m_{ab} = \gamma_{ab} - s_a s_b = g_{ab} + n_a n_b - s_a s_b. \tag{B1}$$

Next, we define the following two null vectors:

$$k^a \equiv \frac{1}{\sqrt{2}}(n^a + s^a) \quad \text{and} \quad l^a \equiv \frac{1}{\sqrt{2}}(n^a - s^a), \tag{B2}$$

satisfying $k^a k_a = 0$, $m_{ab}k^b = 0$, $l^a l_a = 0$ and $m_{ab}l^b = 0$. These vectors at $\mathcal{S}$ are tangent and future pointing to the null geodesics that emanate from $\mathcal{S}$ and whose projection on Σ_t are orthogonal to $\mathcal{S}$. The normalization is chosen so that $k^a l_a = -1$. The vectors k^a and l^a are tangent to the so-called *outgoing* and *ingoing* null geodesics. From Eqs. (B1) and (B2) one obtains

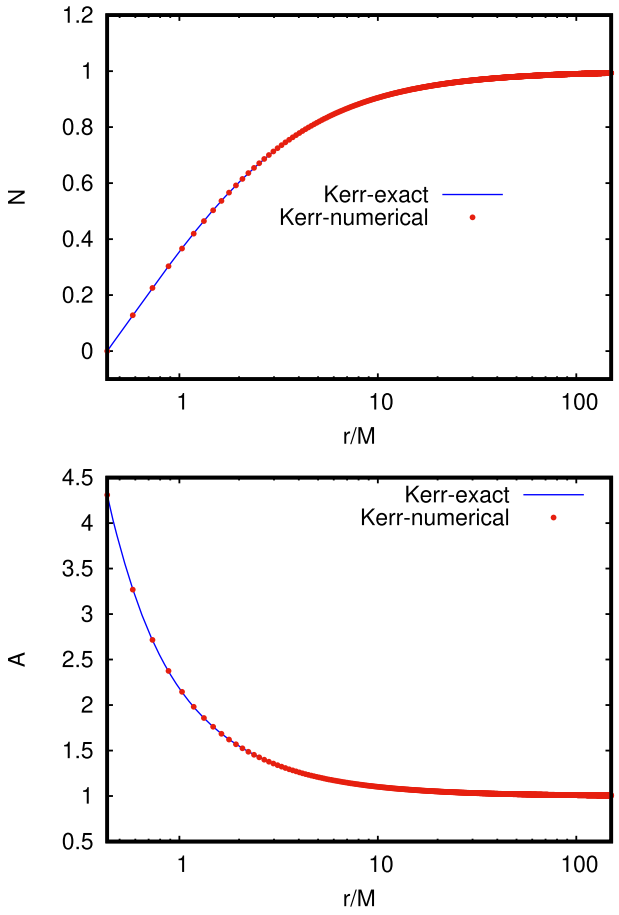

FIG. 18. Red dots correspond to the numerical solution at the equatorial plane ($\theta = \pi/2$) for the lapse function N (top panel) and the metric potential A (bottom panel) obtained from solving the elliptical system using spectral methods (KADATH) and the blue solid lines correspond to the exact Kerr solution taking $a/M = 0.5$.

[10]cf. the notebook https://nbviewer.org/github/sagemanifolds/SageManifolds/blob/master/Notebooks/SM_KerrQI_3p1.ipynb.

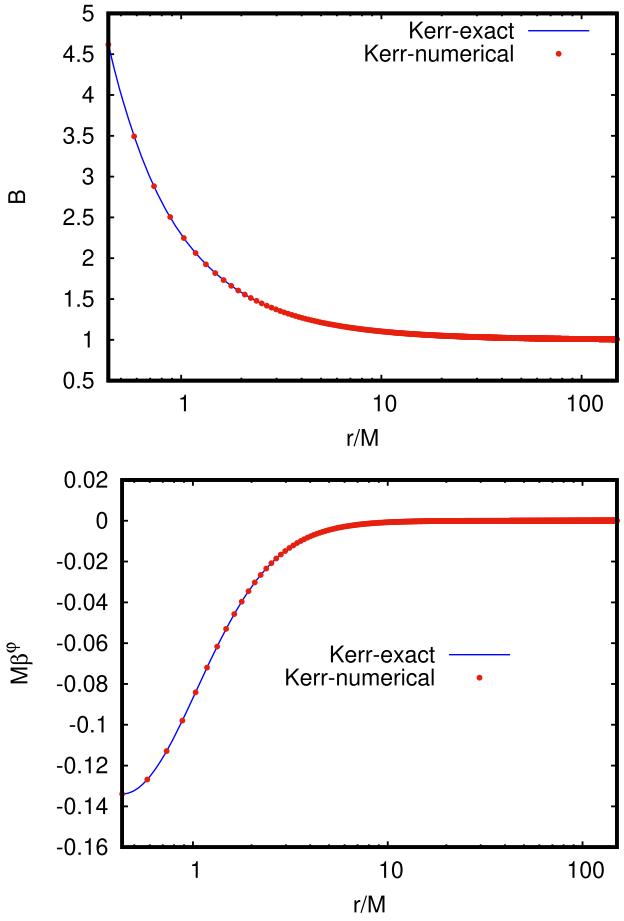

FIG. 19. Similar to Fig. 18 for the metric potential B (top panel) and the shift β^{φ} (bottom panel).

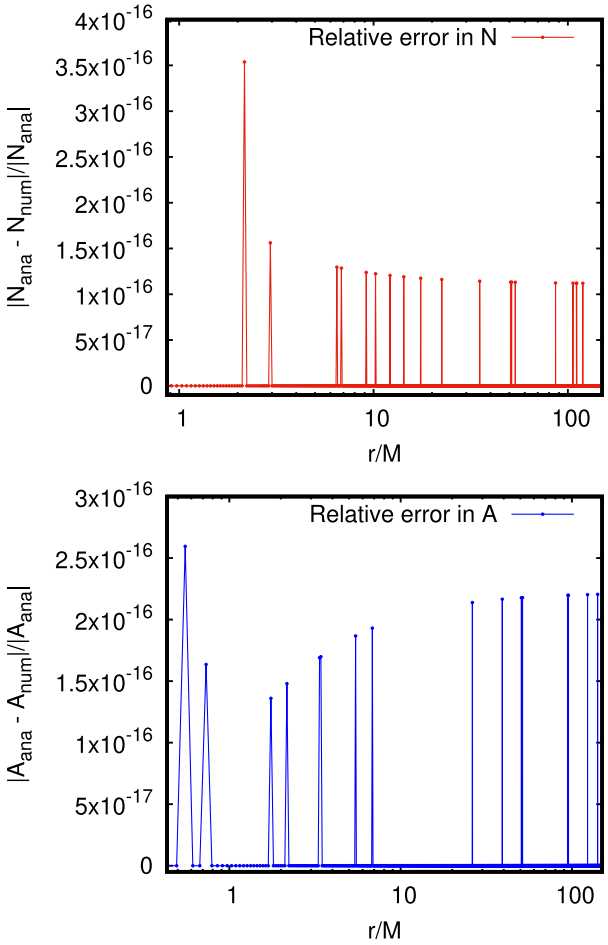

FIG. 20. Relative errors associated with the solutions for N (top panel) and A (bottom panel) shown in Fig. 18.

$$m_{ab} = g_{ab} + k_a l_b + l_a k_b. \tag{B3}$$

The expansion associated with the outgoing null geodesics is defined by

$$H \equiv m^{ab}\nabla_a k_b. \tag{B4}$$

The outer-trapped surface is a surface $\mathcal{S}$ with $H < 0$ and the trapped region is any region of Σ_t containing outer-trapped surfaces. Moreover, when $H = 0$, the surface $\mathcal{S}$ is called *marginally trapped*. The *apparent horizon* is defined as the outermost *marginally trapped surface*. The expansion (B4) can be written in terms of $3+1$ variables as follows [39]:

$$H = D_a s^a - K + K_{ab} s^a s^b. \tag{B5}$$

We can apply this formula to the metric (6), and take as outward-pointing unit (radial) normal $s^a = \frac{1}{A}(\frac{\partial}{\partial r})^a$. Given s^a and since $K_{rr} = 0$, the last term in (B5) vanishes. Moreover, since $K = K^a{}_a = 0$, the expansion is

$$H = D_a s^a = \frac{1}{\sqrt{\gamma}}\partial_r(\sqrt{\gamma}s^r), \tag{B6}$$

where as before $\gamma = A^4 B^2 r^4 \sin^2\theta$ is the determinant of the spatial metric γ_{ab}. In this way, Eq. (B6) reads

$$\begin{aligned} H &= -\frac{1}{A^2}\frac{\partial A}{\partial r} + \frac{1}{A}\left(\frac{2}{A}\frac{\partial A}{\partial r} + \frac{1}{B}\frac{\partial B}{\partial r} + \frac{2}{r}\right) \\ &= \frac{\partial}{\partial r}\left(\frac{1}{A}\right) + \frac{\Gamma}{A}, \end{aligned} \tag{B7}$$

where

$$\Gamma \equiv \left(\frac{2}{A}\frac{\partial A}{\partial r} + \frac{1}{B}\frac{\partial B}{\partial r} + \frac{2}{r}\right). \tag{B8}$$

In Sec. II A Eq. (B7) was used in (23) to impose regularity conditions for the variables A and B at the horizon. For instance, in Kerr spacetime the apparent horizon coincides with the event horizon at $r_H = \sqrt{M^2 - a^2}/2$, and thus

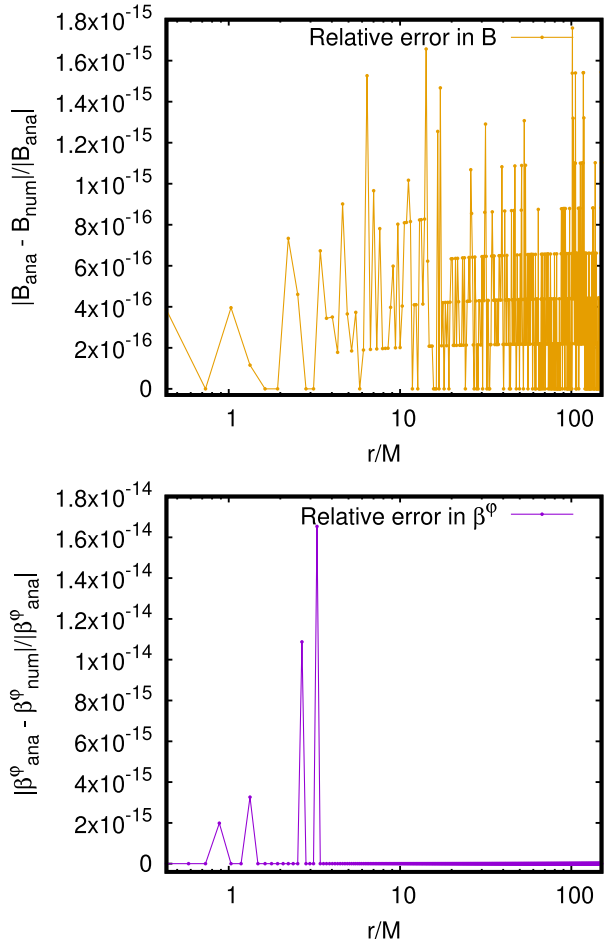

FIG. 21. Relative errors associated with solutions for B (top panel) and β^{φ} (bottom panel) shown in Fig. 19.

$$H|_{r_H} = 0. \tag{B9}$$

We checked using *Mathematica* that the expansion (B7) vanishes at r_H for the Kerr metric in QIC (cf. Appendix A).

APPENDIX C: SURFACE GRAVITY FORMULAS

In order to obtain a simple expression for the surface gravity in terms of derivatives for the lapse function N, the starting point is Eq. (50). That equation leads to [30]

$$\kappa = \lim(V\mathtt{a}) \equiv (V\mathtt{a})_{\mathcal{H}^+}, \tag{C1}$$

where

$$V = (-\chi^a\chi_a)^{1/2}, \tag{C2}$$

$$\mathtt{a} = (a^c a_c)^{1/2}, \tag{C3}$$

$$a^c = \frac{\chi^b\nabla_b\chi^c}{(-\chi^a\chi_a)} = \frac{\chi^b\nabla_b\chi^c}{V^2}. \tag{C4}$$

The vector n^a (29) which is normal to Σ_t is given in terms of the lapse function N and the shift vector β^a as follows [30]:

$$n^a = \frac{1}{N}\left(\frac{\partial}{\partial t}\right)^a - \frac{\beta^i}{N}\left(\frac{\partial}{\partial x^i}\right)^a. \tag{C5}$$

At the horizon and for *axisymmetric* and *circular* spacetime, n^a reduces to (29), and when comparing with (20) we conclude

$$\chi^a = N n^a|_{\mathcal{H}^+}. \tag{C6}$$

Since $n^a n_a = -1$ the squared norm of the helical Killing field is related to the lapse function by

$$-\chi^a\chi_a|_{\mathcal{H}^+} = N^2|_{\mathcal{H}^+} = V^2|_{\mathcal{H}^+} = 0. \tag{C7}$$

Moreover, it is not difficult to prove that the acceleration (C3) of the Killing field χ^a coincides with the acceleration of the normal observers when n^a is given by (C6):

$$\begin{aligned} a^c_{\perp} &= n^a\nabla_a n^c = D^c \ln N, \\ &= \gamma^c_a \nabla^a \ln N, \end{aligned} \tag{C8}$$

as mentioned below Eq. (35), γ^c_a is the *3-metric* (or projector) onto Σ_t and D^c is the covariant derivative compatible with the 3-metric [30,38].

From (C7) and (C8) the surface gravity given by (C1) reads

$$\kappa = [N a_{\perp}]_{\mathcal{H}^+}, \tag{C9}$$

where

$$\begin{aligned} a_{\perp} = \mathtt{a} &= [(D^c \ln N)(D_c \ln N)]^{1/2} \\ &= \left[\frac{\gamma^{ab}}{N^2}(D_a N)(D_b N)\right]^{1/2}. \end{aligned} \tag{C10}$$

The desired formula for the surface gravity in terms of the spatial derivatives of the lapse function and the 3-metric is

$$\begin{aligned} \kappa &= [\gamma^{ab}(D_a N)(D_b N)]^{1/2}_{\mathcal{H}^+} \\ &= \frac{1}{2}\left[\frac{\gamma^{ab}}{N^2}(D_a N^2)(D_b N^2)\right]^{1/2}_{\mathcal{H}^+}. \end{aligned} \tag{C11}$$

When the formula (C11) is applied to the metric (6) one obtains

$$\begin{aligned} \kappa &= \left\{\frac{1}{A}\left[(\partial_r N)^2 + \frac{1}{r^2}(\partial_\theta N)^2\right]^{1/2}\right\}_{r_H} \\ &= \left\{\frac{1}{2AN}\left[(\partial_r N^2)^2 + \frac{1}{r^2}(\partial_\theta N^2)^2\right]^{1/2}\right\}_{r_H}, \end{aligned} \tag{C12}$$

where we used the following expressions for the relevant 3-metric components and its inverse:

$$\gamma_{rr} = A^2, \qquad \gamma_{\theta\theta} = r^2 A^2, \tag{C13}$$

$$\gamma^{rr} = \frac{1}{A^2}, \qquad \gamma^{\theta\theta} = \frac{1}{r^2 A^2}. \tag{C14}$$

For instance, the surface gravity (51) for Schwarzschild and Kerr spacetimes in QIC leads to the well-known expressions [30]:

$$\kappa_{\rm Kerr} = \frac{\sqrt{M^2 - a^2}}{2M(M + \sqrt{M^2 - a^2})}, \tag{C15}$$

$$\kappa_{\rm Schw} = \frac{1}{4M}, \tag{C16}$$

which can be found more straightforwardly in BL coordinates and its nonrotating limit $a = 0$.

APPENDIX D: SCALAR CLOUDS

Using the KADATH library, a code was developed to obtain numerical solutions of *scalar clouds*, which are solutions of Eq. (4) in the background of a Kerr spacetime assuming Eqs. (14) and (26) with an asymptotically vanishing field. These kinds of solution were analyzed thoroughly in Refs. [17,18,20,43] using BL coordinates, and due to the linearity of Eq. (14) one can use separation of variables that leads to Teukolsky equations for the angular $S_{lm}(\theta)$ and radial parts R_{nlm} of the boson field Ψ, which are associated, respectively, with the spheroidal harmonics that depend on the integers l and m ($|m| \leq l$) and the radial function that depends also on the positive integer n (number of nodes). In this context the product $S_{lm}(\theta)R_{nlm}$ (in BL coordinates) is the equivalent of the function $\phi(r, \theta)$ of Eq. (14) (in QI coordinates). Furthermore in Ref. [20] the radial Teukolsky equation is solved using the Kerr parameter a as an *eigenvalue*, so below we report such eigenvalues for the cloud solutions computed here.

We computed scalar clouds using QIC within the aim of using them as input and as initial guess in the spectral code built to find solutions of the full EKG system and thus generate an initial hairy black hole solution. From the latter it was then possible to build a sequence of solutions with the value r_H fixed by varying the frequency Ω_H gradually.

Figures 22 and 23 depict some examples of cloud solutions at the equatorial plane. Although we do not compute hairy solutions for $m > 1$ in this work, for completeness we present cloud solutions for $m = l = 1$, 2, 3.

Tables I–III show the eigenvalues μa that were found for different values of r_H and Ω_H when we solve the Klein-Gordon equation in the background of Kerr spacetime in QI coordinates. The numerical data presented in these tables correspond to configurations with $n = 0$ (nodeless). The results obtained using the spectral code for cloud solutions are consistent with those reported in Ref. [20] for $l = m$ and $n = 0$.

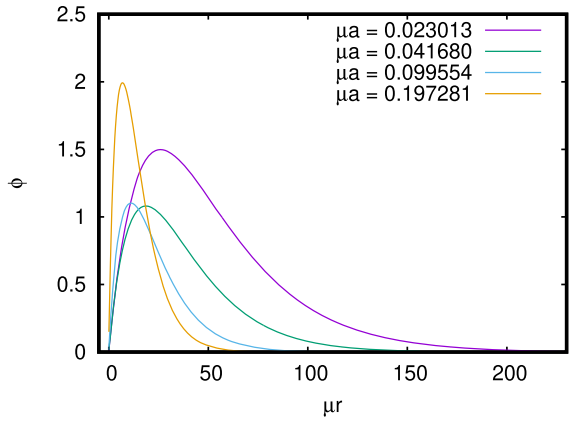

FIG. 22. Scalar clouds around a Kerr black hole in quasi-isotropic coordinates with *quantum numbers* $n = 0$ (nodeless) and $m = l = 1$ (at the equatorial plane $\theta = \pi/2$).

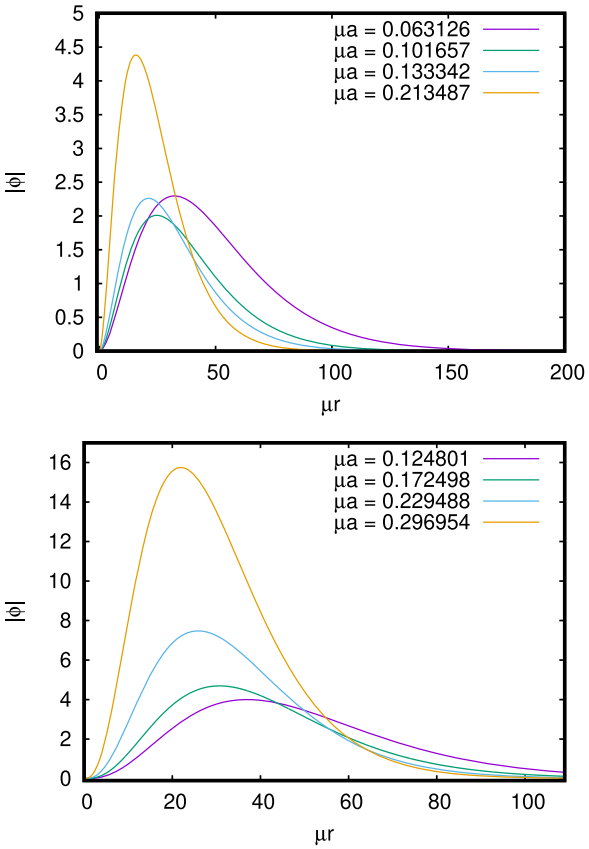

FIG. 23. Scalar clouds around a Kerr black hole in quasi-isotropic coordinates with *quantum numbers* $n = 0$ (nodeless) and integers $m = l = 2$ (top panel), and $m = l = 3$ (bottom panel) respectively (at the equatorial plane $\theta = \pi/2$).

TABLE I. Eigenvalues for a scalar cloud with parameters $m = l = 1$. Some solutions associated with these values appear in Fig. 22.

μR_H	μr_H	μa	μM	Ω_H/μ	a/M
0.15	0.036618	0.023013	0.076766	0.999244	0.299778
0.20	0.047829	0.041680	0.104344	0.998601	0.399449
0.30	0.066740	0.099554	0.166518	0.996433	0.597859
0.40	0.075676	0.197281	0.248650	0.991755	0.793407
0.42	0.074966	0.224626	0.270068	0.990165	0.831739
0.46	0.068260	0.293262	0.323482	0.985409	0.906580
0.48	0.060220	0.338793	0.359564	0.981483	0.942232
0.50	0.045465	0.398850	0.409084	0.974959	0.974984
0.51	0.033064	0.438945	0.443898	0.969403	0.988842
0.52	0.013913	0.491451	0.492238	0.959881	0.998401

TABLE II. Eigenvalues for a scalar cloud with parameters $m = l = 2$. Some solutions associated with these values appear in Fig. 23 (top panel).

μR_H	μr_H	μa	μM	Ω_H/μ	a/M
0.20	0.049490	0.020192	0.101018	0.499733	0.199886
0.35	0.084653	0.063126	0.180692	0.499081	0.349357
0.44	0.104129	0.101657	0.231744	0.498472	0.438660
0.50	0.116110	0.133342	0.267780	0.497954	0.497954
0.62	0.136623	0.213487	0.346756	0.496505	0.615670
0.71	0.147570	0.291552	0.414862	0.494907	0.702769
0.80	0.152408	0.390252	0.495186	0.492558	0.788092
0.92	0.141434	0.570923	0.637156	0.486970	0.896049
1.01	0.104874	0.772441	0.800412	0.477674	0.965054
1.10	0.024718	1.051402	1.052564	0.453219	0.998896

TABLE III. Eigenvalues for a scalar cloud with parameters $m = l = 3$. Some solutions associated with these values appear in Fig. 23 (bottom panel).

μR_H	μr_H	μa	μM	Ω_H/μ	a/M
0.50	0.121336	0.085596	0.257326	0.332636	0.332635
0.60	0.143511	0.124801	0.312980	0.332296	0.398752
0.70	0.164374	0.172498	0.371250	0.331863	0.464640
0.80	0.183543	0.229488	0.432916	0.331311	0.530098
0.90	0.200505	0.296954	0.498990	0.330616	0.595110
1.00	0.214570	0.376460	0.570862	0.329729	0.659459
1.10	0.224748	0.470229	0.650508	0.328574	0.722864
1.20	0.229554	0.581511	0.740902	0.327026	0.784869
1.30	0.226633	0.715231	0.846762	0.324863	0.844666
1.50	0.173267	1.048926	1.104686	0.327146	0.949524

APPENDIX E: HAIRY BLACK HOLE PROPERTIES

Tables IV–IX display some properties of hairy black holes associated with the numerical solutions of the Einstein-Klein-Gordon system discussed in Sec. IV.

TABLE IV. Global quantities and parameters associated with a sequence of rotating hairy black holes with an event horizon located at $\mu r_H = 0.065804$. The columns correspond, respectively, to the angular velocity Ω_H (in units of μ), the ADM mass $M_{\rm ADM} = M_{\rm K}$ (in units of $1/\mu$), the angular momentum J_∞ (in units of $1/\mu^2$), the percentage of the BH mass (at the horizon) relative to the total mass, the percentage of the hair contribution to the total mass, the BH and hair masses $M_{\rm BH}$ and M_Ψ (in units of $1/\mu$) defined as $M^{\mathcal{H}^+}$ and M^{Σ_t} in Sec. III, the BH and hair angular momenta $J_{\rm BH}$ and J_Ψ (in units of $1/\mu^2$) defined as $J^{\mathcal{H}^+}$ and J^{Σ_t} in Sec. III, the total boson number $\mathcal{Q}$ (in units of $1/\mu^2$), the dimensionless ratio $q = m\mathcal{Q}/J_{\rm K}$, the surface gravity κ (in units of μ), and the dimensionless parameter $J_\infty/M^2_{\rm ADM}$. Note that in these examples $J_\Psi = \mathcal{Q}$ (taking $\hbar = 1$) since throughout this work we take the azimuthal number $m = 1$ [cf. Eq. (47)].

Ω_H/μ	$\mu M_{\rm ADM}$	$\mu^2 J_\infty$	$M_{\rm BH}(\%)$	$M_\Psi(\%)$	$\mu M_{\rm BH}$	μM_Ψ	$\mu^2 J_{\rm BH}$	$\mu^2 J_\Psi$	$\mu^2\mathcal{Q}$	q	κ/μ	$J_\infty/M^2_{\rm ADM}$
0.92988	0.81204	0.63310	27.4350	72.5650	0.22278	0.58926	0.04947	0.58363	0.58363	0.92186	0.67177	0.9601
0.93018	0.80851	0.62792	27.9207	72.0793	0.22574	0.58277	0.05104	0.57688	0.57688	0.91871	0.65875	0.9606
0.93078	0.80279	0.61994	28.6299	71.3702	0.22984	0.57295	0.05320	0.56674	0.56674	0.91418	0.64185	0.9619
0.93137	0.79774	0.61315	29.2102	70.7900	0.23302	0.56472	0.05487	0.55828	0.55828	0.91051	0.62954	0.9635
0.93316	0.78405	0.59545	30.6678	69.3326	0.24045	0.54360	0.05873	0.53673	0.53673	0.90138	0.60325	0.9686
0.93494	0.77126	0.57951	31.9509	68.0498	0.24643	0.52484	0.06179	0.51772	0.51772	0.89338	0.58424	0.9742
0.93673	0.75883	0.56435	33.1642	66.8369	0.25166	0.50718	0.06444	0.49991	0.49991	0.88581	0.56894	0.9801
0.93852	0.74655	0.54961	34.3487	65.6529	0.25643	0.49013	0.06684	0.48278	0.48278	0.87839	0.55596	0.9862
0.94030	0.73428	0.53510	35.5265	64.4756	0.26086	0.47343	0.06905	0.46606	0.46605	0.87096	0.54462	0.9925
0.94150	0.72608	0.52549	36.3152	63.6873	0.26368	0.46242	0.07044	0.45505	0.45505	0.86596	0.53777	0.9968
0.94269	0.71784	0.51590	37.1107	62.8922	0.26640	0.45146	0.07178	0.44413	0.44413	0.86087	0.53138	1.0012
0.94388	0.70955	0.50632	37.9157	62.0877	0.26903	0.44054	0.07307	0.43325	0.43325	0.85569	0.52539	1.0057
0.94507	0.70119	0.49671	38.7332	61.2715	0.27159	0.42963	0.07432	0.42240	0.42239	0.85038	0.51975	1.0103
0.94626	0.69277	0.48707	39.5647	60.4401	0.27409	0.41871	0.07553	0.41155	0.41155	0.84493	0.51442	1.0149
0.94745	0.68426	0.47740	40.4131	59.5920	0.27653	0.40776	0.07671	0.40069	0.40069	0.83932	0.50936	1.0196
0.94864	0.67567	0.46766	41.2803	58.7247	0.27892	0.39678	0.07786	0.38980	0.38980	0.83352	0.50455	1.0244
0.94983	0.66697	0.45786	42.1689	57.8360	0.28126	0.38575	0.07898	0.37888	0.37888	0.82750	0.49996	1.0292
0.95103	0.65818	0.44798	43.0808	56.9235	0.28355	0.37466	0.08008	0.36791	0.36791	0.82125	0.49558	1.0341
0.95222	0.64927	0.43802	44.0187	55.9849	0.28580	0.36349	0.08115	0.35687	0.35687	0.81474	0.49139	1.0391
0.95341	0.64025	0.42797	44.9849	55.0173	0.28801	0.35225	0.08220	0.34577	0.34577	0.80793	0.48736	1.0440
0.95460	0.63110	0.41781	45.9822	54.0182	0.29019	0.34091	0.08323	0.33458	0.33458	0.80079	0.48350	1.0490
0.95579	0.62182	0.40754	47.0133	52.9847	0.29234	0.32947	0.08425	0.32330	0.32330	0.79328	0.47978	1.0540
0.95698	0.61239	0.39716	48.0814	51.9135	0.29445	0.31792	0.08525	0.31191	0.31191	0.78536	0.47620	1.0590
0.95817	0.60283	0.38665	49.1897	50.8011	0.29653	0.30624	0.08623	0.30042	0.30042	0.77698	0.47275	1.0640
0.95936	0.59310	0.37600	50.3420	49.6441	0.29858	0.29444	0.08720	0.28880	0.28880	0.76808	0.46942	1.0689
0.96055	0.58322	0.36521	51.5422	48.4378	0.30060	0.28250	0.08816	0.27705	0.27705	0.75861	0.46620	1.0737
0.96175	0.57316	0.35426	52.7952	47.1786	0.30260	0.27041	0.08910	0.26516	0.26516	0.74849	0.46308	1.0784
0.96294	0.56292	0.34315	54.1058	45.8615	0.30457	0.25816	0.09003	0.25313	0.25312	0.73765	0.46007	1.0829
0.96413	0.55248	0.33187	55.4799	44.4812	0.30652	0.24575	0.09094	0.24093	0.24093	0.72598	0.45716	1.0873
0.96532	0.54185	0.32041	56.9237	43.0318	0.30844	0.23317	0.09184	0.22857	0.22857	0.71337	0.45433	1.0913
0.96651	0.53099	0.30876	58.4446	41.5069	0.31034	0.22040	0.09272	0.21604	0.21604	0.69971	0.45159	1.0951
0.96770	0.51991	0.29690	60.0511	39.8994	0.31221	0.20744	0.09358	0.20332	0.20332	0.68483	0.44893	1.0984
0.96889	0.50858	0.28482	61.7524	38.2011	0.31406	0.19429	0.09440	0.19042	0.19042	0.66855	0.44635	1.1012
0.97008	0.49700	0.27252	63.5594	36.4027	0.31589	0.18092	0.09520	0.17732	0.17732	0.65066	0.44385	1.1033
0.97128	0.48515	0.25997	65.4846	34.4931	0.31770	0.16734	0.09597	0.16401	0.16401	0.63086	0.44142	1.1045
0.97247	0.47302	0.24717	67.5419	32.4590	0.31949	0.15354	0.09669	0.15048	0.15048	0.60881	0.43906	1.1047
0.97366	0.46059	0.23409	69.7474	30.2842	0.32125	0.13949	0.09738	0.13671	0.13671	0.58402	0.43677	1.1035
0.97425	0.45426	0.22744	70.9117	29.1379	0.32212	0.13236	0.09771	0.12974	0.12973	0.57040	0.43565	1.1022
0.97485	0.44785	0.22072	72.1200	27.9484	0.32299	0.12517	0.09803	0.12269	0.12269	0.55586	0.43454	1.1005
0.97544	0.44136	0.21392	73.3756	26.7126	0.32385	0.11790	0.09835	0.11557	0.11557	0.54025	0.43345	1.0981
0.97604	0.43479	0.20704	74.6812	25.4264	0.32471	0.11055	0.09866	0.10838	0.10837	0.52345	0.43238	1.0952
0.97664	0.42814	0.20007	76.0405	24.0859	0.32556	0.10312	0.09898	0.10110	0.10110	0.50530	0.43132	1.0915
0.97723	0.42141	0.19302	77.4568	22.6862	0.32641	0.09560	0.09929	0.09373	0.09373	0.48559	0.43028	1.0869
0.97783	0.41458	0.18588	78.9343	21.2222	0.32725	0.08798	0.09962	0.08627	0.08627	0.46410	0.42925	1.0815
0.97842	0.40767	0.17865	80.4776	19.6881	0.32808	0.08026	0.09995	0.07870	0.07870	0.44054	0.42824	1.0749

TABLE V. Global quantities and parameters associated with a sequence of hairy black holes with horizon at $\mu r_H = 0.063567$. The description of columns are like in Table IV.

Ω_H/μ	$\mu M_{\rm ADM}$	$\mu^2 J_\infty$	$M_{\rm BH}(\%)$	$M_\Psi(\%)$	$\mu M_{\rm BH}$	μM_Ψ	$\mu^2 J_{\rm BH}$	$\mu^2 J_\Psi$	$\mu^2 \mathcal{Q}$	q	κ/μ	$J_\infty/M_{\rm ADM}^2$
0.91781	0.86192	0.68500	25.7905	74.2090	0.22229	0.63962	0.05246	0.63254	0.63254	0.92342	0.62823	0.92206
0.92070	0.84161	0.65793	27.8515	72.1483	0.23440	0.60720	0.05883	0.59910	0.59910	0.91058	0.58459	0.92889
0.92359	0.82356	0.63511	29.5362	70.4637	0.24325	0.58031	0.06340	0.57171	0.57171	0.90018	0.55770	0.93638
0.92648	0.80613	0.61368	31.1157	68.8844	0.25083	0.55530	0.06725	0.54643	0.54642	0.89041	0.53729	0.94435
0.92938	0.78883	0.59285	32.6670	67.3333	0.25769	0.53114	0.07069	0.52216	0.52216	0.88076	0.52059	0.95275
0.93227	0.77142	0.57224	34.2286	65.7723	0.26405	0.50738	0.07385	0.49839	0.49839	0.87095	0.50636	0.96159
0.93516	0.75378	0.55163	35.8257	64.1759	0.27005	0.48375	0.07679	0.47484	0.47484	0.86080	0.49392	0.97085
0.93805	0.73579	0.53086	37.4786	62.5243	0.27576	0.46005	0.07956	0.45130	0.45130	0.85013	0.48286	0.98056
0.93921	0.72848	0.52249	38.1594	61.8439	0.27798	0.45052	0.08063	0.44186	0.44186	0.84568	0.47876	0.98455
0.94036	0.72110	0.51406	38.8532	61.1504	0.28017	0.44095	0.08168	0.43238	0.43238	0.84111	0.47482	0.98862
0.94152	0.71364	0.50558	39.5612	60.4427	0.28232	0.43134	0.08271	0.42287	0.42287	0.83641	0.47102	0.99274
0.94267	0.70609	0.49704	40.2846	59.7196	0.28445	0.42168	0.08372	0.41332	0.41332	0.83157	0.46737	0.99693
0.94383	0.69846	0.48842	41.0247	58.9797	0.28654	0.41195	0.08471	0.40372	0.40372	0.82656	0.46384	1.00118
0.94499	0.69074	0.47974	41.7827	58.2218	0.28861	0.40216	0.08569	0.39406	0.39405	0.82139	0.46043	1.00549
0.94614	0.68292	0.47098	42.5601	57.4443	0.29065	0.39230	0.08665	0.38433	0.38433	0.81602	0.45714	1.00986
0.94730	0.67501	0.46214	43.3583	56.6459	0.29267	0.38236	0.08760	0.37454	0.37454	0.81045	0.45395	1.01428
0.94846	0.66698	0.45320	44.1787	55.8249	0.29466	0.37234	0.08853	0.36467	0.36467	0.80465	0.45087	1.01874
0.94961	0.65885	0.44418	45.0233	54.9796	0.29664	0.36224	0.08946	0.35472	0.35472	0.79861	0.44788	1.02325
0.95077	0.65061	0.43505	45.8935	54.1081	0.29859	0.35203	0.09037	0.34469	0.34469	0.79229	0.44497	1.02777
0.95193	0.64225	0.42583	46.7916	53.2085	0.30052	0.34173	0.09126	0.33457	0.33457	0.78568	0.44216	1.03234
0.95308	0.63377	0.41649	47.7193	52.2786	0.30243	0.33133	0.09215	0.32434	0.32434	0.77875	0.43942	1.03691
0.95424	0.62516	0.40704	48.6790	51.3162	0.30432	0.32081	0.09303	0.31401	0.31401	0.77145	0.43676	1.04148
0.95540	0.61642	0.39746	49.6732	50.3187	0.30619	0.31017	0.09390	0.30357	0.30357	0.76376	0.43417	1.04605
0.95655	0.60753	0.38776	50.7045	49.2833	0.30805	0.29941	0.09476	0.29301	0.29301	0.75564	0.43166	1.05058
0.95771	0.59851	0.37793	51.7760	48.2072	0.30988	0.28852	0.09561	0.28233	0.28233	0.74703	0.42921	1.05506
0.95887	0.58933	0.36796	52.8908	47.0868	0.31170	0.27750	0.09645	0.27152	0.27152	0.73789	0.42682	1.05947
0.96002	0.57999	0.35785	54.0527	45.9192	0.31350	0.26633	0.09728	0.26057	0.26057	0.72815	0.42450	1.06380
0.96118	0.57049	0.34758	55.2659	44.7004	0.31528	0.25501	0.09810	0.24948	0.24948	0.71776	0.42224	1.06799
0.96233	0.56081	0.33716	56.5349	43.4262	0.31705	0.24354	0.09892	0.23824	0.23824	0.70662	0.42003	1.07204
0.96349	0.55094	0.32656	57.8647	42.0920	0.31880	0.23190	0.09972	0.22685	0.22685	0.69465	0.41788	1.07586
0.96465	0.54088	0.31580	59.2613	40.6928	0.32054	0.22010	0.10050	0.21530	0.21529	0.68175	0.41578	1.07944
0.96580	0.53062	0.30484	60.7309	39.2229	0.32225	0.20813	0.10127	0.20358	0.20358	0.66780	0.41374	1.08269
0.96696	0.52015	0.29370	62.2809	37.6761	0.32395	0.19597	0.10202	0.19168	0.19168	0.65265	0.41174	1.08555
0.96812	0.50945	0.28235	63.9195	36.0450	0.32564	0.18363	0.10274	0.17961	0.17961	0.63613	0.40979	1.08790
0.96927	0.49852	0.27079	65.6564	34.3214	0.32731	0.17110	0.10343	0.16736	0.16736	0.61803	0.40789	1.08962
0.97043	0.48733	0.25900	67.5017	32.4954	0.32896	0.15836	0.10410	0.15491	0.15490	0.59808	0.40604	1.09057
0.97159	0.47590	0.24698	69.4676	30.5550	0.33059	0.14541	0.10473	0.14225	0.14225	0.57594	0.40423	1.09052
0.97274	0.46420	0.23470	71.5675	28.4859	0.33221	0.13223	0.10534	0.12936	0.12936	0.55118	0.40246	1.08921
0.97390	0.45222	0.22216	73.8172	26.2704	0.33382	0.11880	0.10592	0.11624	0.11624	0.52321	0.40074	1.08633
0.97506	0.43997	0.20934	76.2343	23.8866	0.33540	0.10509	0.10650	0.10284	0.10284	0.49126	0.39906	1.08146
0.97621	0.42741	0.19621	78.8401	21.3080	0.33697	0.09107	0.10708	0.08913	0.08913	0.45427	0.39741	1.07406
0.97737	0.41456	0.18277	81.6599	18.5021	0.33853	0.07670	0.10769	0.07508	0.07508	0.41079	0.39581	1.06349
0.97852	0.40137	0.16898	84.7247	15.4311	0.34006	0.06194	0.10835	0.06063	0.06063	0.35881	0.39425	1.04893
0.97968	0.38783	0.15483	88.0747	12.0506	0.34158	0.04674	0.10907	0.04576	0.04576	0.29552	0.39273	1.02937
0.98084	0.37388	0.14028	91.7606	8.3133	0.34308	0.03108	0.10985	0.03043	0.03043	0.21692	0.39125	1.00351
0.98199	0.35947	0.12530	95.8506	4.1692	0.34456	0.01499	0.11063	0.01467	0.01467	0.11708	0.38980	0.96968

TABLE VI. Global quantities and parameters associated with a sequence of hairy black holes with horizon at $\mu r_H = 0.060889$. The description of columns are like in Table IV.

Ω_H/μ	$\mu M_{\rm ADM}$	$\mu^2 J_\infty$	$M_{\rm BH}(\%)$	$M_\Psi(\%)$	$\mu M_{\rm BH}$	μM_Ψ	$\mu^2 J_{\rm BH}$	$\mu^2 J_\Psi$	$\mu^2 \mathcal{Q}$	q	κ/μ	$J_\infty/M^2_{\rm ADM}$
0.90155	0.92761	0.76171	22.2587	77.7410	0.20647	0.72114	0.04785	0.71386	0.71386	0.93718	0.64054	0.88522
0.90659	0.89423	0.71549	25.5517	74.4479	0.22849	0.66574	0.05965	0.65584	0.65584	0.91663	0.55779	0.89476
0.91276	0.86166	0.67409	28.4042	71.5955	0.24475	0.61691	0.06806	0.60603	0.60603	0.89904	0.51331	0.90792
0.91836	0.83278	0.63880	30.8748	69.1252	0.25712	0.57566	0.07429	0.56451	0.56451	0.88370	0.48560	0.92111
0.92340	0.80636	0.60733	33.1416	66.8588	0.26724	0.53912	0.07929	0.52804	0.52804	0.86944	0.46589	0.93404
0.92845	0.77911	0.57548	35.5181	64.4831	0.27673	0.50239	0.08390	0.49158	0.49158	0.85421	0.44939	0.94806
0.93013	0.76979	0.56471	36.3443	63.6572	0.27977	0.49003	0.08537	0.47935	0.47935	0.84884	0.44443	0.95298
0.93293	0.75394	0.54653	37.7680	62.2342	0.28475	0.46921	0.08774	0.45879	0.45879	0.83947	0.43668	0.96146
0.93573	0.73768	0.52801	39.2588	60.7441	0.28960	0.44810	0.09003	0.43798	0.43798	0.82949	0.42948	0.97030
0.93853	0.72095	0.50911	40.8278	59.1755	0.29435	0.42663	0.09226	0.41686	0.41686	0.81880	0.42278	0.97948
0.94133	0.70372	0.48978	42.4878	57.5159	0.29899	0.40475	0.09441	0.39537	0.39537	0.80724	0.41650	0.98901
0.94414	0.68594	0.46996	44.2529	55.7501	0.30355	0.38241	0.09651	0.37345	0.37345	0.79464	0.41061	0.99884
0.94694	0.66755	0.44961	46.1402	53.8608	0.30801	0.35955	0.09856	0.35105	0.35105	0.78079	0.40506	1.00894
0.95030	0.64464	0.42441	48.5944	51.4011	0.31326	0.33135	0.10096	0.32345	0.32345	0.76212	0.39882	1.02130
0.95198	0.63280	0.41145	49.9114	50.0800	0.31584	0.31690	0.10213	0.30932	0.30932	0.75178	0.39586	1.02752
0.95366	0.62068	0.39825	51.2965	48.6895	0.31839	0.30221	0.10330	0.29495	0.29495	0.74063	0.39299	1.03374
0.95534	0.60828	0.38477	52.7571	47.2225	0.32091	0.28725	0.10444	0.28033	0.28033	0.72856	0.39021	1.03990
0.95702	0.59558	0.37102	54.3017	45.6709	0.32341	0.27201	0.10558	0.26544	0.26544	0.71545	0.38753	1.04595
0.95870	0.58255	0.35696	55.9400	44.0253	0.32588	0.25647	0.10669	0.25027	0.25027	0.70111	0.38492	1.05184
0.96039	0.56918	0.34259	57.6836	42.2757	0.32832	0.24062	0.10779	0.23480	0.23480	0.68537	0.38240	1.05749
0.96207	0.55543	0.32788	59.5459	40.4101	0.33074	0.22445	0.10886	0.21901	0.21901	0.66798	0.37995	1.06278
0.96375	0.54129	0.31281	61.5426	38.4149	0.33313	0.20794	0.10990	0.20290	0.20290	0.64865	0.37758	1.06760
0.96543	0.52673	0.29735	63.6923	36.2741	0.33549	0.19107	0.11091	0.18645	0.18645	0.62702	0.37529	1.07174
0.96711	0.51172	0.28149	66.0166	33.9681	0.33782	0.17382	0.11186	0.16963	0.16963	0.60262	0.37306	1.07496
0.96879	0.49624	0.26519	68.5414	31.4727	0.34013	0.15618	0.11276	0.15243	0.15243	0.57480	0.37090	1.07689
0.96935	0.49096	0.25965	69.4328	30.5937	0.34089	0.15020	0.11304	0.14660	0.14660	0.56463	0.37019	1.07717
0.96991	0.48564	0.25406	70.3509	29.6889	0.34165	0.14418	0.11333	0.14073	0.14073	0.55394	0.36950	1.07723
0.97047	0.48025	0.24841	71.2972	28.7568	0.34241	0.13810	0.11360	0.13481	0.13481	0.54269	0.36880	1.07705
0.97103	0.47481	0.24271	72.2731	27.7957	0.34316	0.13198	0.11387	0.12884	0.12883	0.53082	0.36812	1.07659
0.97159	0.46930	0.23695	73.2801	26.8040	0.34391	0.12579	0.11414	0.12281	0.12281	0.51829	0.36744	1.07583
0.97215	0.46374	0.23113	74.3202	25.7794	0.34465	0.11955	0.11441	0.11672	0.11672	0.50501	0.36678	1.07473
0.97271	0.45812	0.22525	75.3943	24.7200	0.34540	0.11325	0.11467	0.11058	0.11058	0.49091	0.36611	1.07325
0.97327	0.45244	0.21930	76.5050	23.6234	0.34614	0.10688	0.11494	0.10437	0.10437	0.47591	0.36546	1.07135
0.97383	0.44669	0.21329	77.6539	22.4869	0.34687	0.10045	0.11520	0.09809	0.09809	0.45989	0.36481	1.06897
0.97439	0.44088	0.20722	78.8436	21.3078	0.34761	0.09394	0.11547	0.09175	0.09175	0.44275	0.36417	1.06608
0.97495	0.43501	0.20108	80.0758	20.0828	0.34833	0.08736	0.11575	0.08533	0.08533	0.42435	0.36353	1.06260
0.97551	0.42907	0.19486	81.3541	18.8088	0.34906	0.08070	0.11604	0.07883	0.07883	0.40454	0.36291	1.05849
0.97607	0.42305	0.18858	82.6806	17.4822	0.34978	0.07396	0.11633	0.07225	0.07225	0.38312	0.36229	1.05366
0.97663	0.41697	0.18222	84.0589	16.0993	0.35050	0.06713	0.11664	0.06558	0.06558	0.35990	0.36167	1.04803
0.97720	0.41082	0.17578	85.4926	14.6560	0.35122	0.06021	0.11696	0.05882	0.05882	0.33464	0.36106	1.04154
0.97776	0.40458	0.16926	86.9859	13.1483	0.35193	0.05320	0.11729	0.05197	0.05197	0.30706	0.36046	1.03407
0.97832	0.39827	0.16266	88.5432	11.5717	0.35264	0.04609	0.11764	0.04503	0.04503	0.27682	0.35987	1.02552
0.97888	0.39186	0.15598	90.1698	9.9219	0.35334	0.03888	0.11799	0.03799	0.03799	0.24354	0.35928	1.01578
0.97944	0.38537	0.14921	91.8719	8.1945	0.35404	0.03158	0.11836	0.03085	0.03085	0.20678	0.35870	1.00472
0.98000	0.37877	0.14235	93.6555	6.3854	0.35474	0.02419	0.11872	0.02363	0.02363	0.16600	0.35813	0.99218
0.98145	0.36113	0.12408	98.7263	1.2725	0.35653	0.00460	0.11959	0.00449	0.00449	0.03617	0.35667	0.95142

TABLE VII. Global quantities and parameters associated with a sequence of hairy black holes with horizon at $\mu r_H = 0.057648$. The description of columns are like in Table IV.

Ω_H/μ	$\mu M_{\rm ADM}$	$\mu^2 J_\infty$	$M_{\rm BH}(\%)$	$M_\Psi(\%)$	$\mu M_{\rm BH}$	μM_Ψ	$\mu^2 J_{\rm BH}$	$\mu^2 J_\Psi$	$\mu^2 \mathcal{Q}$	q	κ/μ	$J_\infty/M^2_{\rm ADM}$
0.88289	0.98692	0.83265	19.2715	80.7280	0.19019	0.79672	0.04364	0.78901	0.78901	0.94760	0.64591	0.85487
0.88831	0.95134	0.78110	22.7088	77.2908	0.21604	0.73530	0.05785	0.72325	0.72325	0.92590	0.54137	0.86304
0.89372	0.92642	0.74810	24.8664	75.1332	0.23037	0.69605	0.06541	0.68269	0.68269	0.91260	0.50110	0.87166
0.89914	0.90275	0.71795	26.8647	73.1351	0.24252	0.66023	0.07168	0.64627	0.64627	0.90020	0.47300	0.88096
0.90456	0.87915	0.68869	28.8414	71.1583	0.25356	0.62559	0.07725	0.61144	0.61144	0.88780	0.45108	0.89104
0.90997	0.85509	0.65952	30.8603	69.1395	0.26388	0.59121	0.08237	0.57715	0.57715	0.87510	0.43304	0.90199
0.91539	0.83024	0.62995	32.9655	67.0344	0.27369	0.55655	0.08716	0.54279	0.54279	0.86160	0.41771	0.91390
0.92081	0.80434	0.59964	35.1965	64.8036	0.28310	0.52124	0.09167	0.50797	0.50797	0.84710	0.40440	0.92687
0.92622	0.77717	0.56833	37.5945	62.4057	0.29217	0.48500	0.09596	0.47237	0.47237	0.83120	0.39267	0.94095
0.93164	0.74851	0.53575	40.2075	59.7926	0.30096	0.44756	0.10004	0.43570	0.43570	0.81330	0.38220	0.95622
0.93705	0.71815	0.50165	43.0954	56.9048	0.30949	0.40866	0.10395	0.39770	0.39770	0.79280	0.37279	0.97269
0.94247	0.68582	0.46578	46.3358	53.6644	0.31778	0.36804	0.10769	0.35809	0.35809	0.76880	0.36428	0.99029
0.94789	0.65125	0.42784	50.0344	49.9659	0.32585	0.32540	0.11128	0.31657	0.31656	0.73990	0.35653	1.00878
0.95330	0.61407	0.38748	54.3405	45.6600	0.33369	0.28039	0.11471	0.27277	0.27277	0.70400	0.34945	1.02756
0.95872	0.57388	0.34427	59.4744	40.5262	0.34131	0.23257	0.11799	0.22627	0.22627	0.65730	0.34297	1.04535
0.96414	0.53011	0.29767	65.7786	34.2222	0.34870	0.18142	0.12113	0.17654	0.17654	0.59310	0.33704	1.05924
0.96955	0.48205	0.24696	73.8205	26.1805	0.35585	0.12620	0.12410	0.12285	0.12285	0.49750	0.33161	1.06278
0.97497	0.42865	0.19112	84.6222	15.3793	0.36274	0.06592	0.12692	0.06421	0.06421	0.33590	0.32665	1.04017
0.97551	0.42297	0.18521	85.9187	14.0827	0.36341	0.05957	0.12719	0.05802	0.05802	0.31330	0.32618	1.03524
0.97605	0.41721	0.17922	87.2645	12.7370	0.36408	0.05314	0.12746	0.05176	0.05176	0.28880	0.32572	1.02962
0.97660	0.41139	0.17317	88.6627	11.3388	0.36475	0.04665	0.12773	0.04544	0.04544	0.26240	0.32526	1.02322
0.97714	0.40548	0.16704	90.1166	9.8847	0.36541	0.04008	0.12800	0.03905	0.03905	0.23380	0.32480	1.01596
0.97768	0.39951	0.16084	91.6304	8.3711	0.36607	0.03344	0.12826	0.03258	0.03258	0.20260	0.32435	1.00775
0.97822	0.39345	0.15457	93.2080	6.7937	0.36673	0.02673	0.12852	0.02604	0.02604	0.16850	0.32390	0.99846
0.97876	0.38731	0.14821	94.8538	5.1478	0.36738	0.01994	0.12878	0.01943	0.01943	0.13110	0.32346	0.98799
0.97930	0.38109	0.14178	96.5726	3.4286	0.36803	0.01307	0.12904	0.01273	0.01273	0.08980	0.32302	0.97619
0.97985	0.37474	0.13520	98.3856	1.6161	0.36869	0.00606	0.12930	0.00590	0.00590	0.04370	0.32258	0.96281
0.98020	0.37063	0.13096	99.5876	0.4142	0.36910	0.00154	0.12947	0.00150	0.00150	0.01140	0.32231	0.95338

TABLE VIII. Global quantities and parameters associated with a sequence of hairy black holes with horizon at $\mu r_H = 0.053651$. The description of columns are like in Table IV.

Ω_H/μ	$\mu M_{\rm ADM}$	$\mu^2 J_\infty$	$M_{\rm BH}(\%)$	$M_\Psi(\%)$	$\mu M_{\rm BH}$	μM_Ψ	$\mu^2 J_{\rm BH}$	$\mu^2 J_\Psi$	$\mu^2 \mathcal{Q}$	q	κ/μ	$J_\infty/M^2_{\rm ADM}$
0.86072	1.03651	0.89289	16.8732	83.1265	0.17489	0.86162	0.04098	0.85191	0.85191	0.95411	0.62906	0.83109
0.86150	1.02755	0.87878	17.7308	82.2690	0.18219	0.84536	0.04518	0.83361	0.83361	0.94859	0.59177	0.83229
0.86228	1.02214	0.87057	18.2294	81.7704	0.18633	0.83581	0.04752	0.82305	0.82305	0.94541	0.57330	0.83327
0.87011	0.98697	0.82044	21.3387	78.6612	0.21061	0.77636	0.06089	0.75954	0.75954	0.92578	0.49086	0.84224
0.87794	0.95828	0.78209	23.8120	76.1879	0.22819	0.73010	0.07020	0.71190	0.71190	0.91025	0.44892	0.85166
0.88577	0.93038	0.74623	26.1956	73.8043	0.24372	0.68666	0.07818	0.66806	0.66805	0.89524	0.41942	0.86209
0.89360	0.90188	0.71072	28.6221	71.3779	0.25814	0.64374	0.08540	0.62532	0.62532	0.87984	0.39655	0.87378
0.90143	0.87205	0.67451	31.1686	68.8316	0.27181	0.60025	0.09210	0.58241	0.58241	0.86346	0.37790	0.88696
0.91708	0.80641	0.59740	36.8987	63.1033	0.29755	0.50887	0.10430	0.49310	0.49310	0.82541	0.34877	0.91866
0.92961	0.74612	0.52888	42.4793	57.5232	0.31695	0.42919	0.11315	0.41573	0.41573	0.78606	0.33071	0.95003
0.94213	0.67661	0.45179	49.5690	50.4171	0.33539	0.34113	0.12134	0.33044	0.33044	0.73142	0.31587	0.98685
0.95309	0.60581	0.37495	57.8986	42.0604	0.35076	0.25481	0.12803	0.24692	0.24692	0.65855	0.30495	1.02162
0.95936	0.55981	0.32594	64.1638	35.8367	0.35920	0.20062	0.13144	0.19450	0.19450	0.59674	0.29943	1.04006
0.96562	0.50880	0.27226	72.2019	27.9330	0.36736	0.14212	0.13435	0.13792	0.13792	0.50655	0.29439	1.05170
0.96718	0.49519	0.25798	74.5892	25.5800	0.36936	0.12667	0.13503	0.12295	0.12295	0.47660	0.29320	1.05207
0.96875	0.48122	0.24332	77.1652	23.0263	0.37134	0.11081	0.13573	0.10759	0.10759	0.44216	0.29204	1.05072
0.97058	0.46445	0.22569	80.4438	19.7474	0.37362	0.09172	0.13662	0.08908	0.08908	0.39468	0.29072	1.04628
0.97162	0.45461	0.21535	82.4684	17.7059	0.37491	0.08049	0.13717	0.07819	0.07819	0.36306	0.28998	1.04200
0.97266	0.44458	0.20480	84.6180	15.5260	0.37619	0.06902	0.13775	0.06705	0.06705	0.32740	0.28926	1.03621

(Table continued)

TABLE VIII. *(Continued)*

Ω_H/μ	$\mu M_{\rm ADM}$	$\mu^2 J_\infty$	$M_{\rm BH}(\%)$	$M_\Psi(\%)$	$\mu M_{\rm BH}$	μM_Ψ	$\mu^2 J_{\rm BH}$	$\mu^2 J_\Psi$	$\mu^2 \mathcal{Q}$	q	κ/μ	$J_\infty/M_{\rm ADM}^2$
0.97371	0.43432	0.19404	86.9081	13.1940	0.37746	0.05730	0.13837	0.05567	0.05567	0.28689	0.28855	1.02864
0.97475	0.42383	0.18305	89.3570	10.6957	0.37873	0.04533	0.13901	0.04404	0.04404	0.24057	0.28785	1.01899
0.97553	0.41579	0.17465	91.3115	8.7046	0.37966	0.03619	0.13949	0.03516	0.03516	0.20129	0.28733	1.01021
0.97632	0.40758	0.16610	93.3795	6.6060	0.38060	0.02692	0.13996	0.02615	0.02615	0.15743	0.28682	0.99989
0.97710	0.39920	0.15742	95.5735	4.3948	0.38153	0.01754	0.14038	0.01704	0.01704	0.10822	0.28632	0.98782
0.97746	0.39522	0.15331	96.6445	3.3227	0.38196	0.01313	0.14056	0.01275	0.01275	0.08316	0.28609	0.98151
0.97757	0.39407	0.15213	96.9562	3.0116	0.38208	0.01187	0.14061	0.01152	0.01152	0.07574	0.28602	0.97963
0.97767	0.39293	0.15095	97.2706	2.6984	0.38220	0.01060	0.14066	0.01029	0.01029	0.06819	0.28595	0.97770
0.97778	0.39178	0.14976	97.5877	2.3830	0.38232	0.00934	0.14070	0.00906	0.00906	0.06052	0.28589	0.97574
0.97788	0.39062	0.14858	97.9075	2.0656	0.38245	0.00807	0.14074	0.00783	0.00783	0.05272	0.28582	0.97373
0.97799	0.38946	0.14739	98.2297	1.7464	0.38257	0.00680	0.14079	0.00660	0.00660	0.04480	0.28576	0.97168
0.97809	0.38830	0.14619	98.5563	1.4226	0.38269	0.00552	0.14083	0.00536	0.00536	0.03668	0.28569	0.96959
0.97820	0.38713	0.14499	98.8849	1.0982	0.38282	0.00425	0.14087	0.00413	0.00413	0.02846	0.28563	0.96746
0.97830	0.38596	0.14380	99.2155	0.7726	0.38294	0.00298	0.14090	0.00290	0.00289	0.02013	0.28556	0.96529
0.97835	0.38538	0.14320	99.3810	0.6107	0.38300	0.00235	0.14092	0.00228	0.00228	0.01595	0.28553	0.96419
0.97840	0.38479	0.14259	99.5504	0.4424	0.38306	0.00170	0.14094	0.00165	0.00165	0.01159	0.28550	0.96305

TABLE IX. Global quantities and parameters associated with a sequence of hairy black holes with horizon at $\mu r_H = 0.048574$. The description of columns are like in Table IV.

Ω_H/μ	$\mu M_{\rm ADM}$	$\mu^2 J_\infty$	$M_{\rm BH}(\%)$	$M_\Psi(\%)$	$\mu M_{\rm BH}$	μM_Ψ	$\mu^2 J_{\rm BH}$	$\mu^2 J_\Psi$	$\mu^2 \mathcal{Q}$	q	κ/μ	$J_\infty/M_{\rm ADM}^2$
0.83330	1.07819	0.94723	14.3146	85.6853	0.15434	0.92385	0.03672	0.91051	0.91051	0.96123	0.61389	0.81482
0.83365	1.07215	0.93753	14.8114	85.1885	0.15880	0.91335	0.03940	0.89814	0.89814	0.95798	0.58745	0.81560
0.83540	1.05970	0.91812	15.8508	84.1491	0.16797	0.89173	0.04479	0.87334	0.87334	0.95122	0.54214	0.81759
0.83991	1.04067	0.88954	17.4979	82.5019	0.18210	0.85857	0.05286	0.83668	0.83668	0.94057	0.48880	0.82137
0.84441	1.02576	0.86791	18.8317	81.1682	0.19317	0.83259	0.05903	0.80889	0.80888	0.93199	0.45626	0.82486
0.84891	1.01229	0.84887	20.0589	79.9410	0.20305	0.80924	0.06442	0.78444	0.78444	0.92411	0.43200	0.82838
0.85342	0.99947	0.83114	21.2382	78.7617	0.21227	0.78720	0.06937	0.76177	0.76177	0.91654	0.41247	0.83202
0.85792	0.98691	0.81412	22.3971	77.6028	0.22104	0.76587	0.07400	0.74012	0.74012	0.90910	0.39608	0.83586
0.86243	0.97440	0.79748	23.5519	76.4481	0.22949	0.74491	0.07840	0.71908	0.71908	0.90169	0.38196	0.83993
0.86843	0.95753	0.77548	25.1039	74.8960	0.24038	0.71715	0.08399	0.69149	0.69149	0.89170	0.36576	0.84580
0.87444	0.94021	0.75336	26.6885	73.3116	0.25093	0.68928	0.08930	0.66405	0.66405	0.88146	0.35182	0.85222
0.88044	0.92225	0.73085	28.3226	71.6775	0.26121	0.66105	0.09440	0.63645	0.63645	0.87084	0.33962	0.85927
0.88645	0.90349	0.70774	30.0227	69.9778	0.27125	0.63224	0.09930	0.60844	0.60844	0.85970	0.32881	0.86703
0.89246	0.88377	0.68386	31.8058	68.1949	0.28109	0.60268	0.10402	0.57984	0.57984	0.84789	0.31914	0.87557
0.89846	0.86296	0.65903	33.6912	66.3101	0.29074	0.57223	0.10859	0.55045	0.55045	0.83524	0.31041	0.88497
0.90447	0.84091	0.63311	35.7010	64.3009	0.30021	0.54072	0.11300	0.52011	0.52011	0.82152	0.30248	0.89531
0.91047	0.81749	0.60592	37.8620	62.1404	0.30952	0.50799	0.11726	0.48866	0.48866	0.80648	0.29524	0.90667
0.91648	0.79254	0.57732	40.2074	59.7955	0.31866	0.47390	0.12139	0.45594	0.45593	0.78974	0.28861	0.91913
0.92148	0.77046	0.55227	42.3316	57.6685	0.32615	0.44431	0.12473	0.42754	0.42754	0.77416	0.28348	0.93037
0.92549	0.75187	0.53136	44.1639	55.8324	0.33206	0.41979	0.12734	0.40402	0.40402	0.76035	0.27962	0.93993
0.92949	0.73240	0.50960	46.1347	53.8553	0.33789	0.39444	0.12990	0.37970	0.37970	0.74509	0.27597	0.95001
0.93350	0.71197	0.48691	48.2675	51.7133	0.34365	0.36818	0.13241	0.35451	0.35451	0.72806	0.27249	0.96058
0.93750	0.69048	0.46324	50.5920	49.3782	0.34933	0.34095	0.13487	0.32837	0.32837	0.70885	0.26919	0.97163
0.94150	0.66783	0.43848	53.1460	46.8158	0.35493	0.31265	0.13727	0.30121	0.30121	0.68694	0.26606	0.98313
0.94551	0.64390	0.41253	55.9783	43.9848	0.36044	0.28322	0.13959	0.27295	0.27295	0.66164	0.26307	0.99500
0.94951	0.61852	0.38528	59.1528	40.8329	0.36587	0.25256	0.14178	0.24351	0.24351	0.63203	0.26024	1.00709
0.95352	0.59156	0.35659	62.7514	37.2895	0.37122	0.22059	0.14379	0.21280	0.21280	0.59677	0.25754	1.01898
0.95602	0.57385	0.33786	65.2614	34.8317	0.37450	0.19988	0.14495	0.19291	0.19291	0.57097	0.25593	1.02596
0.95802	0.55919	0.32238	67.4383	32.7025	0.37711	0.18287	0.14583	0.17655	0.17655	0.54765	0.25468	1.03098
0.96002	0.54408	0.30645	69.7850	30.4025	0.37969	0.16541	0.14669	0.15977	0.15976	0.52134	0.25345	1.03522
0.96202	0.52852	0.29003	72.3226	27.9006	0.38224	0.14746	0.14755	0.14248	0.14248	0.49126	0.25226	1.03830

(Table continued)

TABLE IX. *(Continued)*

Ω_H/μ	$\mu M_{\rm ADM}$	$\mu^2 J_\infty$	$M_{\rm BH}(\%)$	$M_\Psi(\%)$	$\mu M_{\rm BH}$	μM_Ψ	$\mu^2 J_{\rm BH}$	$\mu^2 J_\Psi$	$\mu^2 \mathcal{Q}$	q	κ/μ	$J_\infty/M_{\rm ADM}^2$
0.96403	0.51249	0.27309	75.0770	25.1586	0.38477	0.12894	0.14846	0.12463	0.12463	0.45636	0.25111	1.03976
0.96603	0.49598	0.25560	78.0811	22.1306	0.38726	0.10976	0.14947	0.10613	0.10613	0.41522	0.24998	1.03904
0.96803	0.47891	0.23750	81.3795	18.7640	0.38973	0.08986	0.15060	0.08690	0.08690	0.36590	0.24889	1.03551
0.97003	0.46119	0.21875	85.0339	15.0031	0.39217	0.06919	0.15184	0.06691	0.06691	0.30587	0.24782	1.02845
0.97203	0.44269	0.19930	89.1310	10.7926	0.39457	0.04778	0.15311	0.04619	0.04619	0.23174	0.24679	1.01695
0.97403	0.42323	0.17907	93.7895	6.08030	0.39694	0.02573	0.15421	0.02486	0.02486	0.13883	0.24579	0.99972
0.97604	0.40266	0.15800	99.1603	0.80870	0.39928	0.00326	0.15486	0.00314	0.00314	0.01990	0.24483	0.97451

TABLE X. Thermodynamic properties associated with a hairy black hole with horizon at $\mu r_H = 0.057648$.

Ω_H/μ	$\mu M_{\rm ADM}$	$\mu^2 J_\infty$	κ/μ	T_H/μ	$\mu^2 \mathcal{A}$	$\mu^2 S_H$	$\mu M_{\rm Smarr}$
0.88289	0.986917	0.832652	0.645915	0.102801	2.20098	0.55024	0.986913
0.88831	0.951343	0.781093	0.541370	0.086162	2.62930	0.65732	0.951340
0.89373	0.926418	0.748099	0.501102	0.079753	2.84506	0.71126	0.926414
0.89914	0.902750	0.717944	0.472997	0.075280	3.01884	0.75471	0.902749
0.90456	0.879152	0.688689	0.451077	0.071791	3.17039	0.79260	0.879150
0.90997	0.855091	0.659515	0.433038	0.068920	3.30730	0.82683	0.855089
0.91539	0.830236	0.629945	0.417709	0.066481	3.43346	0.85837	0.830235
0.92081	0.804335	0.599639	0.404400	0.064362	3.55113	0.88778	0.804335
0.92622	0.777166	0.568322	0.392667	0.062495	3.66175	0.91544	0.777167
0.93164	0.748513	0.535743	0.382205	0.060830	3.76631	0.94158	0.748514
0.93706	0.718148	0.501651	0.372796	0.059332	3.86549	0.96632	0.718150
0.94247	0.685822	0.465783	0.364277	0.057977	3.95975	0.98994	0.685823
0.94789	0.651244	0.427841	0.356527	0.056743	4.04944	1.01236	0.651246
0.95331	0.614070	0.387477	0.349450	0.055617	4.13478	1.03369	0.614073
0.95872	0.573875	0.344266	0.342973	0.054586	4.21589	1.05397	0.573878
0.96414	0.530110	0.297665	0.337040	0.053642	4.29282	1.07320	0.530115
0.96956	0.482045	0.246955	0.331609	0.052777	4.36551	1.09138	0.482050
0.97497	0.428652	0.191123	0.326653	0.051989	4.43378	1.10845	0.428658
0.97551	0.422967	0.185206	0.326183	0.051914	4.44036	1.11009	0.422973
0.97606	0.417212	0.179221	0.325718	0.051840	4.44688	1.11172	0.417218
0.97660	0.411385	0.173167	0.325257	0.051766	4.45336	1.11334	0.411391
0.97714	0.405485	0.167041	0.324800	0.051694	4.45979	1.11495	0.405490
0.97768	0.399507	0.160841	0.324348	0.051622	4.46617	1.11654	0.399513
0.97822	0.393451	0.154566	0.323901	0.051551	4.47251	1.11813	0.393457
0.97876	0.387314	0.148211	0.323459	0.051480	4.47879	1.11970	0.387320
0.97931	0.381095	0.141775	0.323021	0.051410	4.48502	1.12125	0.381099
0.97985	0.374785	0.135256	0.322588	0.051341	4.49120	1.12280	0.374793
0.98020	0.370630	0.130963	0.322308	0.051297	4.49519	1.12380	0.370636

[1] W. Israel, Phys. Rev. **164**, 1776 (1967); Commun. Math. Phys. **8**, 245 (1968); B. Carter, Phys. Rev. Lett. **26**, 331 (1971); R. Wald, Phys. Rev. Lett. **26**, 1653 (1971); D. C. Robinson, Phys. Rev. Lett. **34**, 905 (1975); P. Q. Mazur, J. Phys. A **15**, 3173 (1982); Phys. Lett. **100A**, 341 (1984).

[2] B. Carter, Phys. Rev. **174**, 1559 (1968).

[3] J. E. Chase, Commun. Math. Phys. **19**, 276 (1970); J. D. Bekenstein, Phys. Rev. Lett. **28**, 452 (1972); Phys. Rev. D **5**, 1239 (1972); **5**, 2403 (1972); J. B. Hartle, in *Magic Without Magic*, edited by J. Klauder (Freeman, San Francisco, 1972); C. Teitelboim, Phys. Rev. D **5**, 2441 (1972); M. Heusler, J. Math. Phys. (N.Y.) **33**, 3497 (1992); J. D. Bekenstein, Phys. Rev. D **51**, R6608 (1995).

[4] D. Sudarsky, Classical Quantum Gravity **12**, 579 (1995).

[5] I. Peña and D. Sudarsky, Classical Quantum Gravity **14**, 3131 (1997).

[6] B. C. Xanthopoulos and T. Zannias, J. Math. Phys. (N.Y.) **32**, 1875 (1991); A. Saa, Phys. Rev. D **53**, 7377 (1996); J. Math. Phys. (N.Y.) **37**, 2346 (1996); A. E. Mayo and J. D. Bekenstein, Phys. Rev. D **54**, 5059 (1996); E. Ayon-Beato, Classical Quantum Gravity **19**, 5465 (2002).

[7] https://pnp.ligo.org/ppcomm/Papers.html.

[8] A. M. Ghez, B. L. Klein, M. Morris, and E. E. Becklin, Astrophys. J. **509**, 678 (1998); A. M. Ghez, M. Morris, and E. E. Becklin, A. Tanner, and T. Kremenek, Nature (London) **407**, 349 (2000); A. M. Ghez *et al.*, Astrophys. J. **586**, L127 (2003); **689**, 1044 (2008).

[9] A. Eckart and R. Genzel, Nature (London) **383**, 415 (1996); R. Abuter *et al.* (Gravity Collaboration), Astron. Astrophys. **615**, L15 (2018).

[10] K. Akiyama *et al.* (The event Horizon Telescope Collaboration), Astrophys. J. Lett. **875**, L1 (2019); **910**, L12 (2021).

[11] R. D. Blanford and R. L. Znajek, Mon. Not. R. Astron. Soc. **179**, 433 (1977); S. S. Doeleman *et al.*, Science **338**, 355 (2022).

[12] P. Bizon and T. Chmaj, Phys. Lett. B **297**, 55 (1992); M. Heusler, S. Droz, and N. Straumann, Phys. Lett. B **268**, 371 (1991); **271**, 61 (1991); **285**, 21 (1992); P. Bizon, Phys. Rev. Lett. **64**, 2844 (1990); M. S. Volkov and D. V. Gal'tsov, Sov. J. Nucl. Phys. **51**, 747 (1990); H. P. Künzle and A. K. M. Masood-ul Alam, J. Math. Phys. (N.Y.) **31**, 928 (1990); B. R. Greene, S. D. Mathur, and C. M. O'Neill, Phys. Rev. D **47**, 2242 (1993); G. Lavrelashvili and D. Maison, Nucl. Phys. **B410**, 407 (1993); O. Bechmann and O. Lechtenfeld, Classical Quantum Gravity **12**, 1473 (1995); H. Dennhardt and O. Lechtenfeld, Int. J. Mod. Phys. A **13**, 741 (1998); B. Kleihaus, J. Kunz, and F. Navarro-Lérida, Classical Quantum Gravity **33**, 234002 (2016); C. Herdeiro, E. Radu, and H. Rúnarsson, Classical Quantum Gravity **33**, 154001 (2016).

[13] U. Nucamendi and M. Salgado, Phys. Rev. D **68**, 044026 (2003).

[14] M. S. Volkov and D. V. Gal'tsov, Phys. Rep. **319**, 1 (1999); M. S. Volkov, Hairy black holes in the XX-th and XXI-st century, *Proceedings of the MG14 Meeting on General Relativity*, edited by M. Bianchi, R. T. Jantzen, and R. Ruffini (World Scientific, Singapore, 2018).

[15] https://iopscience.iop.org/journal/02649381/page/Focusissueonhairyblackholes.

[16] N. Straumann and Z.-H. Zhou, Phys. Lett. B **243**, 33 (1990); Z.-H. Zhou and N. Straumann, Nucl. Phys. **B360**, 180 (1991); P. Bizon, Phys. Lett. B **259**, 53 (1991); P. Bizon and R. M. Wald, Phys. Lett. B **267**, 173 (1991); R. M. Wald, J. Math. Phys. (N.Y.) **33**, 248 (1992); O. Brodbeck and N. Straumann, J. Math. Phys. (N.Y.) **37**, 1414 (1996).

[17] C. Herdeiro and E. Radu, Phys. Rev. Lett. **112**, 221101 (2014).

[18] C. Herdeiro and E. Radu, Classical Quantum Gravity **32**, 144001 (2015).

[19] C. Benone, L. C. B. Crispino, C. Herdeiro, and E. Radu, Phys. Rev. D **90**, 104024 (2014).

[20] G. García and M. Salgado, Phys. Rev. D **99**, 044036 (2019).

[21] G. García and M. Salgado, Phys. Rev. D **101**, 044040 (2020).

[22] B. Ganchev and J. E. Santos, Phys. Rev. Lett. **120**, 171101 (2018).

[23] J. C. Degollado, C. A. R. Herdeiro, and E. Radu, Phys. Lett. B **781**, 651 (2018).

[24] B. Kleihaus, J. Kunz, and S. Yazadjiev, Phys. Lett. B **744**, 406 (2015); H. Motohashi and M. Minamitsuji, Phys. Rev. D **99**, 064040 (2019); M. Minamitsuji and J. Edholm, Phys. Rev. D **100**, 044053 (2019); C. Charmousis, M. Crisostomi, R. Gregory, and N. Stergioulas, Phys. Rev. D **100**, 084020 (2019); K. Takahashi and H. Motohashi, J. Cosmol. Astropart. Phys. 06 (2020) 034; J. Achour, H. Liu, and S. Mukohyama, J. Cosmol. Astropart. Phys. 02 (2020) 023; E. Babichev, C. Charmousis, A. Cisterna, and M. Hassaine, J. Cosmol. Astropart. Phys. 06 (2020) 049; K. V. Aelst, E. Gourgoulhon, P. Grandclément, and C. Charmousis, Classical Quantum Gravity **37**, 035007 (2020); J. Achour, H. Liu, H. Motohashi, S. Mukohyama, and K. Noui, J. Cosmol. Astropart. Phys. 11 (2020) 001; R. Benkel, T. P. Sotiriou, and H. Witek, Phys. Rev. D **94**, 121503(R) (2016); H. Witek, L. Gualtieri, P. Pani, and T. P. Sotiriou, Phys. Rev. D **99**, 064035 (2019); F. L. Julié, H. O. Silva, E. Berti, and N. Yunes, Phys. Rev. D **105**, 124031 (2022); F. L. Julié, H. O. Silva, E. Berti, N. Yunes, A. Hegade K. R., E. R. Most, J. Noronha, H. Witek, and N. Yunes, Phys. Rev. D **105**, 064041 (2022); D. Langlois, K. Noui, and H. Roussille, Phys. Rev. D **104**, 124044 (2021); J. Cosmol. Astropart. Phys. 09 (2022) 019; arXiv:2205.07746.

[25] F. Long, S. Chen, M. Wang, and J. Jing, Eur. Phys. J. C **80**, 1180 (2020); B. Shiralilou, T. Hinderer, S. M. Nissanke, N. Ortiz, and H. Witek, Phys. Rev. D **103**, L121503 (2021); Classical Quantum Gravity **39**, 035002 (2022); H. O. Silva, H. Witek, M. Elley, and N. Yunes, Phys. Rev. Lett. **127**, 031101 (2021); N. Loutrel and N. Yunes, Phys. Rev. D **106**, 064009 (2022); J. Dong, N. Patiño, Y. Xie, A. Cárdenas-Avendaño, C. F. Gammie, and N. Yunes, Phys. Rev. D **105**, 044008 (2022).

[26] P. G. S. Fernandes and D. J. Mulryne, arXiv:2212.07293.

[27] P. Grandclément and J. Novak, Living Rev. Relativity **12**, 1 (2009).

[28] P. Grandclément, J. Comput. Phys. **229**, 3334 (2010); https://kadath.obspm.fr.

[29] L. Papenfort, S. Tootle, P. Grandclément, E. Most, and L. Rezzolla, Phys. Rev. D **104**, 024057 (2021).

[30] R. M. Wald, *General Relativity* (Chicago University Press, Chicago, 1984).

[31] A. Papapetrou, Ann. Inst. H. Poincare, A **4**, 83 (1966).

[32] B. Carter, J. Math. Phys. (N.Y.) **10**, 70 (1969).

[33] B. Carter in *Black Holes—Les Houches 1972*, Edited by C. DeWitt and B. S. DeWitt (Gordon & Breach Science Publishers, New York, 1973).

[34] P. Grandclément and J. Nicoules, Phys. Rev. D **105**, 104011 (2022).

[35] E. Gourgoulhon, arXiv:1003.5015.

[36] E. Gourgoulhon, Black hole spacetimes in quasi-isotropic coordinates (unpublished).

[37] P. Grandclément, C. Somé, and E. Gourgoulhon, Phys. Rev. D **90**, 024068 (2014).

[38] E. Gourgoulhon, *3 + 1 Formalism in General Relativity* (Springer, Berlin, 2012).

[39] M. Alcubierre, *Intorduction to 3 + 1 Numerical Relativity* (Oxford University Press, Oxford, 2008).

[40] T. W. Baumgarte and S. L. Shapiro, *Numerical Relativity: Solving Einstein's Equations on the Computer* (Cambridge University Press, New York, 2010).
[41] C. Herdeiro and E. Radu, Int. J. Mod. Phys. D **24**, 1542014 (2015).
[42] I. Smolić, Classical Quantum Gravity **32**, 145010 (2015); Phys. Rev. D **95**, 024016 (2017).
[43] S. Hod, Phys. Rev. D **86**, 104026 (2012); **86**, 129902(E) (2012); Phys. Lett. B **751**, 177 (2015).
[44] S. A. Teukolsky, Phys. Rev. Lett. **29**, 1114 (1972).
[45] S. W. Hawking, Commun. Math. Phys. **25**, 152 (1972); S. W Hawking and G. F. R. Ellis, *The Large Scale Structure of Space Time* (Cambridge University Press, Cambridge, England, 1973).
[46] M. Heusler, *Black Hole Uniqueness Theorems* (Cambridge University Press, Cambridge, England, 1996).
[47] P. Grandclément, G. Fodor, and P. Forgacs, Phys. Rev. D **84**, 065037 (2011).
[48] G. Fodor, P. Forgacs, and P. Grandclément, Phys. Rev. D **89**, 065027 (2014).
[49] F. E. Schunck and E. W. Mielke, Gen. Relativ. Gravit. **31**, 787 (1999); Classical Quantum Gravity **20**, R301 (2003).
[50] J. M. Bardeen, B. Carter, and S. W. Hawking, Commun. Math. Phys. **31**, 161 (1973).
[51] L. Smarr, Phys. Rev. Lett. **30**, 71 (1973); **30**, 521(E) (1973).
[52] P. V. P. Cunha, C. A. R. Herdeiro, E. Radu, and H. F. Rúnarsson, Int. J. Mod. Phys. D **25**, 1641021 (2016); P. V. P. Cunha, J. Grover, C. Herdeiro, E. Radu, H. Rúnarsson, and A. Wittig, Phys. Rev. D **94**, 104023 (2016); F. H. Vincent, E. Gourgoulhon, C. Herdeiro, and E. Radu, Phys. Rev. D **94**, 084045 (2016); P. V. P. Cunha, C. A. R. Herdeiro, and E. Radu, Phys. Rev. D **96**, 024039 (2017).
[53] Y. Ni, M. Zhou, A. Cárdenas-Avendaño, C. Bambi, C. A. R. Herdeiro, and E. Radu, J. Cosmol. Astropart. Phys. 07 (2016) 049; N. Franchini, P. Pani, A. Maselli, L. Gualtieri, C. A. R. Herdeiro, E. Radu, and V. Ferrari, Phys. Rev. D **95**, 124025 (2017).
[54] https://heasarc.gsfc.nasa.gov/docs/suzaku; https://www.isdc.unige.ch/extp/; M. Feroci *et al.*, Exp. Astron. **34**, 415 (2012).
[55] H. O. Silva, A. Ghosh, and A. Buonanno, Phys. Rev. D **107**, 044030 (2023).
[56] M. Hannam *et al.*, Nature (London) **610**, 652 (2022).